A delta-tubulin/epsilon-tubulin/Ted protein complex is required for centriole architecture

Rachel Pudlowski[1], Lingyi Xu[1], Ljiljana Milenkovic[2], Katherine Hemsworth[1], Tim Stearns[2,3], Jennifer T. Wang[1,*]

1 - Department of Biology, Washington University in St. Louis
2 - Department of Biology, Stanford University
3 - Rockefeller University
* - Corresponding author

Abstract

Centrioles have a unique, conserved architecture formed by three linked “triplet” microtubules arranged in nine-fold symmetry. The mechanisms by which these triplet microtubules are formed are not understood, but likely involve the noncanonical tubulins delta-tubulin and epsilon-tubulin. Previously, we found that human cells deficient in delta-tubulin or epsilon-tubulin form abnormal centrioles, characterized by an absence of triplet microtubules, lack of central core protein POC5, and a futile cycle of centriole formation and disintegration (Wang et al., 2017). Here, we show that human cells lacking either of the associated proteins TEDC1 and TEDC2 have these same phenotypes. Using ultrastructure expansion microscopy, we identified the roles of these proteins and triplet microtubules in centriole architecture by mapping the locations of centriolar proteins throughout the cell cycle. We find that mutant centrioles have normal architecture during S-phase. By G2-phase, mutant centrioles grow to the same length as control centrioles, but fail to recruit inner scaffold proteins of the central core. Instead, the inner lumen of centrioles is filled with an expanded proximal region, indicating that these proteins, or the triplet microtubules themselves, may be required for recruiting central core proteins and restricting the length of the proximal end. During mitosis, the mutant centrioles elongate further before fragmenting and disintegrating. All four proteins physically interact and TEDC1 and TEDC2 are capable of interacting in the absence of the tubulins. These results support an AlphaFold Multimer structural prediction model for the tetrameric complex, in which delta-tubulin and epsilon-tubulin are predicted to form a heterodimer. TEDC1 and TEDC2 localize to centrosomes and are mutually dependent on each other and on delta-tubulin and epsilon-tubulin for localization. These results indicate that delta-tubulin, epsilon-tubulin, TEDC1, and TEDC2 function together in promoting robust centriole architecture. This work also lays the groundwork for future dissection of this complex, which will provide a basis for determining the mechanisms that underlie the assembly and interplay between compound microtubules and inner centriole structure.

Introduction

The major microtubule organizing center of mammalian cells, the centrosome, is composed of two barrel-shaped centrioles surrounded by layers of pericentriolar material (Breslow and Holland, 2019). The unique architecture of the centriole is highly conserved: the centriole barrel walls of approximately 250 nm in diameter by 500 nm in length are formed of compound microtubules linked to each other through shared protofilament walls, arranged in nine-fold symmetry (Wang and Stearns, 2017). Centrioles exhibit proximal-distal polarity comprised of three subdomains: the proximal end with triplet microtubules, the distal end with doublet microtubules, and the central core spanning the two regions (LeGuennec et al., 2021). The triplet microtubules are named the A-, B-, and C-tubules. The A-tubule is a complete microtubule formed of 13 protofilaments, and the B- and C-tubules are partial tubules and share protofilament walls with adjacent tubules. The A- and B-tubules extend beyond the C-tubule to form the doublet microtubules of the centriole distal end. During ciliogenesis, the A- and B-tubules elongate further to form the ciliary axoneme (Wang and Stearns, 2017).

Compound microtubules are unique to centrioles and ciliary axonemes and are conserved in almost all organisms with these organelles. Little is known about the mechanisms by which they form, or the functional roles they play within centrioles and cilia. Two non-canonical members of the tubulin superfamily, delta-tubulin (TUBD1) and epsilon-tubulin (TUBE1), are required for compound microtubule formation or stability in multiple organisms (de Loubresse et al., 2001; Dupuis-Williams et al., 2002; Dutcher and Trabuco, 1998; Dutcher et al., 2002; Gadelha et al., 2006; Goodenough and StClair, 1975; Ross et al., 2013; Wang et al., 2017). Previously, we showed that human cells lacking these tubulins make aberrant centrioles that only have singlet microtubules and disintegrate in mitosis, resulting in a futile cycle of centriole formation and loss every cell cycle (Wang et al., 2017). These mutant centrioles fail to recruit the distal end protein POC5, indicating that compound microtubules may be required for centriole composition. We concluded that either the compound microtubules themselves, or the proteins that they associate with, are required for centriole stability through the cell cycle. Together, these results suggest that the compound microtubules may form a unique scaffold for the protein-protein interactions that define centrosomes and cilia.

Here, we build upon our previous work by addressing two important questions relating to triplet microtubule formation and function. First, are there additional proteins that regulate triplet microtubule formation or stability? Second, how do compound microtubules affect the overall architecture of centrioles?

Toward the first question, two additional proteins, TEDC1 (C14orf80) and TEDC2 (C16ORF59), have been reported to interact with TUBD1 and TUBE1 (Breslow et al., 2018; Huttlin et al., 2017; Huttlin et al., 2021). Loss of TEDC1 or TEDC2 in 3T3 cells results in a variable distribution of centriole numbers through the cell cycle, and tagged TEDC1 localizes to centrosomes (Breslow et al., 2018). Here, we create *Tedc1*$^{-/-}$ or *Tedc2*$^{-/-}$ mutants cells in the same background as the *Tubd1*$^{-/-}$ and *Tube1*$^{-/-}$ mutants and test whether these cells undergo a futile centriole cycle and whether their centrioles may have compound microtubules. We localize

TEDC1 and TEDC2 to centrosomes using both diffraction-limited immunofluorescence and expansion microscopy. In addition, we extend our understanding of the interactions between these four proteins by defining their mutual dependencies, whether any might form subcomplexes within cells, and report an AlphaFold-Multimer structural prediction model for the complex.

Toward the second question, multiple lines of evidence suggest that the compound microtubules may scaffold some of the protein-protein interactions that occur within centrosomes. Electron microscopy and cryo-electron tomography studies have shown that the compound microtubules are directly linked to many of the substructures within centrioles (LeGuennec et al., 2021). At the proximal end, the cartwheel, a ninefold symmetric hub and spokes made from SASS6 and associated proteins, forms early in procentriole biogenesis during G1/S phase. Multiple cartwheels are stacked within the centriole lumen to approximately one-third of the entire centriole length (~170 nm in human centrioles) (Klena et al., 2020). The cartwheel is connected to the A-tubule through the pinhead, which has been proposed to be formed of CEP135 and CPAP (Hatzopoulos et al., 2013; Kraatz et al., 2016; Lin et al., 2013a; Sharma et al., 2016). The cartwheel and centriolar microtubules have been proposed to assemble interdependently to impart ninefold symmetry upon the centriole (Hilbert et al., 2016), but it is unclear how the cartwheel might be regulated in centrioles lacking compound microtubules.

Within the central core, a helical inner scaffold is formed in G2-phase of the first cell cycle after centriole birth, imparts structural integrity upon the centriole (Le Guennec et al., 2020; Steib et al., 2020), and recruits proteins, including gamma-tubulin, to the lumen of the centriole (Schweizer et al., 2021). This scaffold is formed of POC5, POC1B, FAM161A, WDR90, and CCDC15 and contacts all three (A-, B-, and C-) tubules (Arslanhan et al., 2023; Le Guennec et al., 2020; Steib et al., 2020). WDR90 has been proposed to form the inner junction stem bridging the inner scaffold and the interface between the A- and B-tubules (Steib et al., 2020). The distal region of centrioles also has a unique protein composition, including the proteins centrin, CP110, SFI1, CEP97, CEP90, OFD1, and MNR (Kleylein-Sohn et al., 2007; Kumar et al., 2021; Laporte et al., 2022; Le Borgne et al., 2022; Spektor et al., 2007). The connections between the compound microtubules and these distal end proteins are not well-understood.

In addition to scaffolding these architectural substructures within centrioles, compound microtubules may also be involved in recruiting or regulating enzymes that modify centrioles during their maturation. During the first cell cycle after their formation, procentrioles acquire post-translational modifications, elongate, recruit the inner scaffold, lose the cartwheel, and undergo centriole-to-centrosome conversion. Additional changes occur during the second cell cycle, including acquisition of the distal and subdistal appendages that are important for ciliogenesis.

Here, we directly test the scaffolding hypothesis by determining whether loss of the compound microtubules affects the positioning of proteins along the centriole, and the changes that occur to centrioles during the first cell cycle after their formation. We note that due to the futile

127 centriole cycle in these mutant cells, we could only assay centriole architecture during the first
128 cell cycle. In addition, because centrioles are constitutively formed *de novo* every cell cycle in
129 our mutant cells, we incorporated two controls to our analysis: procentrioles undergoing normal
130 parental-mediated centriole duplication in control (RPE-1 *p53*$^{-/-}$) cells, and centrioles formed in
131 RPE-1 *p53*$^{-/-}$ cells *de novo* in the first cell cycle after centrinone washout. The architecture of *de*
132 *novo*-formed centrioles has not been systematically characterized prior to this study, though this
133 mechanism has been shown to be error-prone, perhaps indicating differences in centriole
134 structure or regulation (Wang et al., 2015).
135
136 We find that the compound microtubules are required for recruiting the helical inner scaffold and
137 correctly positioning the proximal end, and dispensable for recruitment of distal end proteins and
138 centriole elongation. In mitosis, mutant centrioles continue elongating before fragmenting and
139 disintegrating. Together, these results indicate that the compound microtubules are required for
140 scaffolding substructures within centrioles and centriole stability through the cell cycle.
141

142 Results

143

144 Loss of TEDC1 or TEDC2 phenocopies loss of TUBD1 or TUBE1

145 Are there additional proteins that regulate compound microtubule formation or stability? TEDC1
146 and TEDC2 have been reported to physically interact with delta-tubulin and epsilon-tubulin, and
147 loss of either *Tedc1* or *Tedc2* in 3T3 cells results in cells with a variable number of centrioles
148 through the cell cycle (Breslow et al., 2018). To further dissect the phenotypes of loss of *Tedc1*
149 or *Tedc2* and directly compare to our original report on delta-tubulin and epsilon-tubulin, we
150 used CRISPR/Cas9 to generate strong loss of function/null mutations in *Tedc1* or *Tedc2* in the
151 same cell type and background genotype (hTERT RPE-1 *p53*$^{-/-}$) as the *Tubd1*$^{-/-}$ (delta-tubulin
152 knockout) and *Tube1*$^{-/-}$ (epsilon-tubulin knockout) mutant cells (Fig 1 - Supp 1). By
153 immunofluorescence staining for two centriolar proteins, centrin and CP110, we observed that
154 *Tedc1*$^{-/-}$ and *Tedc2*$^{-/-}$ mutant cells had similar phenotypes to each other and to *Tubd1*$^{-/-}$ and
155 *Tube1*$^{-/-}$ mutant cells: in an asynchronously growing culture, about half of the cells had no
156 centrioles, and half had five or more centrioles. These phenotypes were fully rescued by
157 expression of tagged TEDC1 (TEDC1-Halotag-3xFlag) or TEDC2 (TEDC2-V5-APEX2) (Fig 1A).
158
159 Next, we checked whether the centrioles in *Tedc1*$^{-/-}$ and *Tedc2*$^{-/-}$ mutant cells underwent a futile
160 cycle of centriole formation and disintegration. We synchronized cells in each stage of the cell
161 cycle, quantified the number of cells with centrioles, and found that almost all mutant cells
162 lacked centrioles in G0/G1 phase. Centrioles formed in S-phase and disintegrated in M (Fig 1B).
163 The centrioles that were present in mutant cells were immature: all centrioles were positive for
164 the procentriole marker SASS6 and negative for the mature centriole marker CEP164 (Fig 1C,
165 1D). We conclude that cells lacking TEDC1 or TEDC2 also undergo a futile cycle, similar to cells
166 lacking delta-tubulin or epsilon-tubulin.
167
168 We also examined the centriolar microtubule status of *Tedc1*$^{-/-}$ and *Tedc2*$^{-/-}$ mutant cells by
169 TEM. Similar to cells lacking delta-tubulin or epsilon-tubulin, we found that centrioles in *Tedc1*$^{-/-}$
170 and *Tedc2*$^{-/-}$ mutant cells lacked compound microtubules and only had singlet microtubules (Fig

171 1E). Together, these results demonstrate that loss of TEDC1 or TEDC2 phenocopies loss of
172 delta-tubulin or epsilon-tubulin, indicating that these proteins likely act together.
173
174 **TEDC1 and TEDC2 localize to centrosomes**
175 Next, we investigated the localization of TEDC1 and TEDC2 to determine if they may directly
176 act on centrosomes. By immunofluorescence, we found that in our rescued cell lines, the tagged
177 rescue constructs localize to centrosomes, (Fig 2A and 2B) and the antibodies for the tags were
178 specific (Fig 2 - Supp Fig 1). TEDC1 and TEDC2 were enriched at centrosomes in S/G2 and
179 colocalized with SASS6, but not centrin, indicating that Tedc1 and Tedc2 may localize to newly
180 formed procentrioles and/or the proximal ends of parental centrioles.
181
182 To analyze TEDC1 and TEDC2 localization at higher resolution, we used ultrastructure
183 expansion microscopy (U-ExM, Gambarotto et al., 2019) to localize our tagged rescue
184 constructs. We found that both proteins localize to procentrioles and the proximal ends of
185 parental centrioles. Within these areas, both proteins show some overlap with the centriolar
186 microtubules. Together, these results show that TEDC1 and TEDC2 localize to centrosomes
187 and likely directly act upon them.
188
189 **TEDC1, TEDC2, TUBD1 and TUBE1 form a complex in cells**
190 To determine how TEDC1, TEDC2, TUBD1 and TUBE1 might act together, we first determined
191 whether they are mutually required for their localization at centrosomes. We found that TEDC1
192 did not localize to centrioles in the absence of TEDC2, TUBD1, or TUBE1 (Figure 3A). Likewise,
193 TEDC2 did not localize to centrioles in the absence of TEDC1, TUBD1, or TUBE1 (Figure 3B).
194 These results indicate that these proteins are mutually required for TEDC1 or TEDC2
195 localization. Furthermore, overexpression of TEDC1 or TEDC2 did not rescue the centriole
196 phenotypes in any of the other mutants, indicating that TEDC1 and TEDC2 are not downstream
197 effectors of TUBD1 and TUBE1 (Fig 3A and 3B).
198
199 TEDC1 and TEDC2 have previously been shown to physically interact with TUBD1 and TUBE1
200 (Breslow et al., 2018). To further probe the nature of this interaction, we first determined
201 whether any of these proteins may form subcomplexes in cells. We expressed TEDC1-Halotag-
202 3xFlag in each mutant cell line and determined whether immunoprecipitation of tagged TEDC1
203 could precipitate the other proteins. TEDC1-Halotag-3xFlag rescuing the *Tedc1*$^{-/-}$ mutant could
204 precipitate TEDC2, TUBD1, and TUBE1, indicating that all four proteins physically interact.
205 TEDC1 did not interact with epsilon-tubulin in the absence of delta-tubulin, nor did it interact with
206 delta-tubulin in the absence of TUBE1. In the absence of TEDC2, TEDC1 did not interact with
207 TUBD1 or TUBE1. However, in the absence of TUBD1 or TUBE1, TEDC1 and TEDC2 could
208 still interact with each other (Fig 3C).
209
210 We performed the reciprocal experiment, in which we expressed TEDC2-V5-APEX2 in each
211 mutant cell line and determined whether immunoprecipitation of tagged TEDC2 could precipitate
212 the other proteins. We observed similar results as our analysis with TEDC1. TEDC2-V5-APEX2
213 rescuing the *Tedc2*$^{-/-}$ mutant could precipitate TEDC1, TUBD1, and TUBE1, indicating that all
214 four proteins physically interact. TEDC2 did not interact with either tubulin in the absence of the

other. In the absence of TEDC1, TEDC2 did not interact with either tubulin. However, in the absence of TUBD1 or TUBE1, TEDC2 and TEDC1 could still interact (Fig 3D).

Together, these experiments indicate that TEDC1, TEDC2, TUBD1 and TUBE1 physically interact with each other, as previously reported (Breslow et al., 2018; Huttlin et al., 2017; Huttlin et al., 2021). Furthermore, TEDC1 and TEDC2 can form a subcomplex in the absence of either tubulin.

To gain additional insight into the nature of this interaction, we used AlphaFold-Multimer (Evans et al., 2021) to predict the structure of the complex. AlphaFold-Multimer predicted that TUBD1 and TUBE1 would form a heterodimer, similar to the alpha-tubulin/beta-tubulin heterodimer, with TUBD1 at the minus-end of the heterodimer. AlphaFold also predicted that the alpha-helices of TEDC1 and TEDC2 interact with each other, and that TEDC1 and TEDC2 form an interaction surface with TUBD1. These predictions, especially at the interface between TEDC1, TEDC2, and TUBD1, yielded high confidence pLDDT and PAE scores (Fig 3E-G). As controls, we used AlphaFold-Multimer to predict whether TEDC1 and TEDC2 might interact with alpha-tubulin and beta-tubulin, and whether similar structures would be predicted for *Xenopus* TEDC1, TEDC2, TUBD1 and TUBE1. While AlphaFold-Multimer did not predict a high-confidence interaction for TEDC1, TEDC2, alpha- and beta-tubulin (Fig 3 - Supp 1 - Fig A-C), it did predict a high-confidence structure for *Xenopus* TEDC1, TEDC2, TUBD1 and TUBE1, similar to that predicted for the human proteins (Fig 3 - Supp 1 - Fig D-F).

Our pulldown experiments showed that TEDC1 and TEDC2 can interact in a subcomplex in the absence of TUBD1 or TUBE1, which supports the predicted structural model, in which TEDC1 and TEDC2 are predicted to directly interact with each other without being bridged by either tubulin. Further supporting this model, immunoprecipitation of TEDC2 identifies the other proteins in stoichiometric amounts (Breslow et al., 2018), and we previously showed that TUBD1 and TUBE1 physically interact (Wang et al., 2017). Future work will be necessary to confirm these structural predictions. Together, these experiments indicate that TEDC1, TEDC2, TUBD1 and TUBE1 physically interact in a complex and are recruited together to centrioles.

Loss of TEDC1, TEDC2, TUBD1 or TUBE1 results in centrioles with aberrant ultrastructure

Next, we determined how the loss of these proteins, and the triplet microtubules themselves, affect centriole ultrastructure and protein composition. We first tested whether mutant centrioles were capable of elongating during the cell cycle. We compared the length of mutant centrioles in all four mutant cell lines to the length of centrioles from two control conditions: procentrioles undergoing normal parental-mediated centriole duplication in control (RPE-1 *p53*$^{-/-}$) cells, and centrioles formed in RPE-1 *p53*$^{-/-}$ cells *de novo* in the first cell cycle after centrinone washout. For each cell line, cells were synchronized by mitotic shake off, resulting in coverslips enriched for cells in S, G2, or M phases. Cells were then expanded by U-ExM and stained for acetylated tubulin to mark centrioles and PCNA to mark S-phase cells. We found that in S-phase, centrioles were short in all conditions. In G2-phase, centrioles elongated in all conditions, and

259 mutant centrioles reached approximately similar lengths as control centrioles (Fig 4A, 4B).
260 These results indicate that centrioles with singlet microtubules can elongate to the same length
261 as controls, and therefore that triplet microtubules are not essential for regulating centriole
262 length. Consistent with this hypothesis, CEP120, a protein involved in regulating centriole length
263 (Comartin et al., 2013; Lin et al., 2013b; Mahjoub et al., 2010), was present and properly
264 localized within mutant centrioles (Fig 4 - Supp 1D).
265
266 We next tested whether the microtubules of mutant centrioles could be modified by post-
267 translational modifications. The compound microtubules of centrioles are heavily post-
268 translationally modified, and recent studies have indicated that each tubule may acquire
269 different modifications (Guichard et al., 2023). We first checked acetylation of alpha-tubulin, one
270 of the most well-studied centriole post-translational modifications. During centriole formation,
271 acetylation is thought to proceed from the proximal toward the distal end and from the A- to the
272 C-tubules (Sahabandu et al., 2019). We found that antibodies against acetylated alpha-tubulin
273 stained mutant centrioles well (Fig 4B), indicating that centrioles with only singlet A-tubules can
274 be acetylated.
275
276 Next, we checked glutamylation, a post-translational modification thought to be restricted to the
277 outer surface of centrioles. Within *Chlamydomonas* centrioles, glutamylation is differentially
278 distributed between each tubule: on the C-tubule at the distal end, on all 3 tubules in the central
279 core, and on the A-tubule at the proximal end. In human centrioles, polyglutamylation is
280 enriched in the proximal and central regions, and is absent in the distal region (Mahecic et al.,
281 2020). We used two antibodies to detect glutamylation: the GT335 antibody, which recognizes
282 the glutamylation branch and thus detects all polyglutamylation, and the polyE antibody, which
283 recognizes long polyglutamate side chains with at least 2 or 3 glutamate residues (Kann et al.,
284 2003; Van Dijk et al., 2007). We found that mutant and control centrioles could be stained by
285 GT335 (Fig 4C), indicating that mutant centrioles are at least mono-glutamylated. However, the
286 polyE antibody did not label control procentrioles, making this antibody uninformative for our
287 mutants (Fig 4D). These results show that centrioles with just singlet microtubules (A-tubules)
288 can be mono-glutamylated. Moreover, our results suggest that centriole glutamylation is a multi-
289 step process, in which long glutamate side chains are added later during centriole maturation.
290
291 We previously demonstrated that *Tubd1*$^{-/-}$ and *Tube1*$^{-/-}$ mutant centrioles fail to recruit the distal
292 centriole protein POC5 (Wang et al., 2017). Using expansion microscopy, we found that *Tedc1*$^{-/-}$
293 and *Tedc2*$^{-/-}$ mutant centrioles also failed to recruit POC5 (Fig 4Ei). Since our original work was
294 published, POC5 was shown to be a component of the helical inner scaffold within the central
295 core. These results indicate that the helical inner scaffold is not properly formed in centrioles
296 with singlet microtubules. To test the mechanisms underlying loss of POC5, we next tested
297 whether mutant centrioles recruit WDR90, which has been proposed to localize to the inner
298 junction between the A- and B-tubules and function in recruiting the inner scaffold (Steib et al.,
299 2020). We found that WDR90 was not recruited to mutant centrioles, in contrast to control
300 centrioles, in which it is recruited in G2-phase (Fig 4Eii). From these results, it is likely that
301 mutant centrioles with singlet microtubules fail to build or stabilize the inner junction between the
302 A- and B-tubules. In the absence of the inner junction and junctional protein WDR90, centrioles

303 with singlet microtubules cannot form the inner scaffold. As a further test of inner scaffold
304 function, we sought to determine whether gamma-tubulin, which is recruited to the lumen of
305 centrioles by the inner scaffold, had localization defects in mutant centrioles. However, we were
306 unable to reliably detect gamma-tubulin within the lumen of control or *de novo*-formed centrioles
307 in S or G2-phase (Fig 4-Supp1E), and thus were unable to test this hypothesis.
308
309 Next, we tested whether the centriole proximal end might be properly formed in mutant
310 centrioles. We found that the centriolar cartwheel protein, SASS6, was present within the lumen
311 of control and mutant procentrioles in S-phase. In control centrioles in G2-phase, SASS6 was
312 restricted to just the proximal end. Surprisingly, SASS6 was elongated throughout the length of
313 the centriole in all G2-phase mutant centrioles (Fig 4F). We observed a similar phenotype with
314 multiple other proximal-end proteins: CEP135, STIL, and CPAP (Fig 4G-I), CEP44 (Fig 4 - Supp
315 1A), indicating that the entire proximal end is elongated in mutant centrioles. The extended
316 localization of proximal end proteins was not due to increased protein expression in mutant cells
317 (Fig 4 - Supp 2). We conclude that loss of TEDC1, TEDC2, TUBD1, or TUBE1 results in
318 elongated proximal end domains that span the length of the mutant centrioles.
319
320 Elongation of the proximal end of centrioles may also indicate an overall defect in centriole
321 polarity. To test this hypothesis, we next determined whether these mutant centrioles might
322 properly recruit proteins to their distal ends. We found that CETN2 and CP110, two proteins of
323 the distal centriole, were localized to mutant centrioles and clearly marked one end of the
324 centriole barrel in both S-phase and G2-phase (Fig 4 - Supp 1B, 1C). We conclude that
325 proximal-to-distal centriole polarity was unaffected in mutant centrioles, and proximal end
326 elongation did not affect the recruitment of proteins to the centriole distal end. Together, these
327 results indicate that centrioles lacking compound microtubules are unable to properly regulate
328 the length of the proximal end.
329
330 **Mutant centrioles elongate further in mitosis before fragmenting**
331
332 Centrioles lacking triplet microtubules undergo a futile cycle of formation and disassembly, but
333 the mechanisms underlying this disassembly are not well-understood. We first tested whether
334 centriole loss in mutant centrioles may be due to loss of CEP295. CEP295 promotes centriole-
335 to-centrosome conversion, a process in which pericentriolar material is recruited to newly-
336 formed procentrioles. Cells lacking CEP295 form centrioles that disintegrate during the cell
337 cycle due to a failure to undergo centriole-to-centrosome conversion (Izquierdo et al., 2014).
338 Using U-ExM, we found that CEP295 was present and normally localized within mutant
339 centrioles in both S- and G2-phases (Fig 4 - Supp 1F). We conclude that centriole loss in our
340 mutants is unlikely due to loss of CEP295 localization, and therefore that TEDC1, TEDC2,
341 TUBD1 and TUBE1 are likely part of a different pathway required for centriole stability through
342 the cell cycle.
343
344 Next, we used U-ExM to visualize centriole loss during mitosis. We stained for the centriole wall
345 (GT335), the centriole proximal end (SASS6) and the centriole distal end (CP110). In control
346 cells, in which centrioles formed *de novo* after centrinone washout, multiple centrioles could be

seen throughout mitosis, and SASS6 was lost from centrioles in anaphase-stage cells (Fig 5A,B). By contrast, in prometaphase stage *Tubd1*$^{-/-}$ or *Tube1*$^{-/-}$ cells, we found that centrioles had a unique appearance: they were longer than normal, with an elongated proximal end marked by SASS6, and a CP110-positive cap. These two ends were connected by weak monoE staining (Fig 5C, 5E). This phenotype is identical to our observations of centrioles in a prometaphase *Tube1*$^{-/-}$ cell by TEM in our previous publication (Wang et al., 2017, Fig 2B), suggesting that this structure may represent an intermediate in the centriole disassembly process.

After metaphase, centrioles in mutant cells were either completely absent, or had a fragmented appearance (Fig 5D, 5F), with aggregates of staining that did not resemble true centrioles. We conclude that in our mutant cells, centriole disassembly likely occurs through centriole elongation and fragmentation, with an aberrant intermediate structure during disassembly.

Discussion

Here, we extend our previous study on delta-tubulin (TUBD1), epsilon-tubulin (TUBE1) and the centriolar triplet microtubules. Previously, we showed that loss of either of these proteins from mammalian cultured cell lines results in the same phenotype: loss of the triplet microtubules and a futile cycle of centriole formation and disintegration (Wang et al., 2017). Here, we add two new proteins to this pathway: TEDC1 and TEDC2, which were originally identified by their association with TUBD1 and TUBE1 (Breslow et al., 2018; Huttlin et al., 2017; Huttlin et al., 2021). Loss of TEDC1 or TEDC2 phenocopies the loss of TUBD1 or TUBE1: aberrant centrioles are formed that lack triplet microtubules and disintegrate during passage through mitosis. TEDC1 and TEDC2 localize to centrioles, indicating that they have a direct role in forming or maintaining centriole structure, and their localization depends on each of the other three proteins within the complex. All four proteins physically interact with each other. Using our mutant cell lines, we interrogated whether any of these proteins can form subcomplexes within cells. We found that TEDC1 and TEDC2 can interact with each other independently of the tubulins, supporting a predicted AlphaFold-Multimer model. Together, these results indicate that these four proteins act together in a complex at centrosomes to form or stabilize the compound microtubules.

Using ultrastructure expansion microscopy, we find that mutant centrioles with singlet microtubules exhibit additional major architectural defects, including absence of the inner scaffold and elongation of the proximal end. We propose that the absence of the inner scaffold arises from the loss of the B- and C-tubules within centrioles, which may serve to anchor WDR90 and/or other proteins of the inner scaffold. WDR90 has been proposed to localize to the inner junction between the A- and B-tubules and is required for recruiting other inner scaffold components (Le Guennec et al., 2020; Steib et al., 2020). We find that mutant centrioles with singlet microtubules fail to localize WDR90, and thus speculate that the B-tubule is required to recruit or stabilize WDR90 at the inner junction. In addition, by cryo-electron tomography, the inner scaffold makes connections to all three (A-, B-, and C-) tubules. Though the identities of all the proteins that form these connections have not been determined, it is possible that mutant

391 centrioles with only A-tubules also fail to provide anchoring sites for the other proteins within the
392 inner scaffold. Together, these results demonstrate that the compound microtubules of
393 centrioles are required for proper formation of the inner helical scaffold of the central core.
394
395 Mutant centrioles with singlet microtubules have an elongated proximal end that extends the
396 entire length of the centriole, as marked by multiple proximal end markers (SASS6, CEP135,
397 STIL, CPAP, CEP44). These results are also supported by our previous observations that by
398 TEM, the lumen of *Tubd1*$^{-/-}$ and *Tube1*$^{-/-}$ mutant centrioles are filled with electron-dense material
399 (Wang et al., 2017). Little is known about the molecular mechanisms that regulate proximal end
400 length, though centrioles from the symbiotic flagellate *Trichonympha* bear an elongated
401 proximal region with extended cartwheel, and the doublet and singlet-bearing centrioles from
402 *Drosophila* and *C. elegans* have cartwheels that extend the entire length of the centriole
403 (González et al., 1998; Guichard and Gönczy, 2016; Guichard et al., 2012; Pelletier et al., 2006;
404 Woglar et al., 2022). We speculate that the triplet microtubules, the inner scaffold, and/or the
405 TUBD1/TUBE1/TEDC1/TEDC2 protein complex might act to limit the length of the proximal end.
406
407 Many aspects of centriole architecture, including centriole length regulation prior to mitosis,
408 acquisition of post-translational modifications, establishment of proximal-distal polarity, and
409 recruitment of proteins required for centriole-to-centrosome conversion, are unaffected in
410 mutant centrioles. These results indicate that the proteins that regulate these processes can act
411 upon the A-tubule independently of the B- and C-tubules.
412
413 Here, we also extend our previous observations of centriole loss in mutant centrioles. In most
414 cell types, centrioles are inherited by daughter cells during each mitosis. Centriole loss is not
415 unique to centrioles lacking compound microtubules: mammalian cells engineered to lack
416 CEP295 also form centrioles that are lost through the cell cycle, due to an inability to undergo
417 centriole to centrosome conversion (Izquierdo et al., 2014). Similarly, in *Drosophila* oocytes,
418 down-regulation of Polo kinase and pericentriolar material triggers centriole elimination
419 (Pimenta-Marques et al., 2016). We find that CEP295 is properly localized in mutant centrioles
420 with singlet microtubules, indicating that centriole loss in this context may be independent of
421 centriole to centrosome conversion and pericentriolar material recruitment. Using expansion
422 microscopy, we find that centriole loss is correlated with loss of the SASS6 cartwheel in mitosis.
423 In this regard, mutant centrioles with singlet microtubules resemble centriole loss within *C.*
424 *elegans* oocytes, in which an analogous structure to the cartwheel named the central tube is lost
425 prior to centriole widening and subsequent loss of the centriolar microtubules (Pierron et al.,
426 2023). In addition, centriole loss in our mutant cells occurs through a stereotyped progression of
427 architectural changes in mitosis, starting with centriole over elongation in prometaphase and
428 culminating with centriole fragmentation and loss. Prolonged mitotic arrest has been reported to
429 result in centriole over elongation through Plk1 activity (Kong et al., 2020), and it is possible that
430 a lengthened mitosis, as observed in these mutant cells and cells lacking centrioles (Farrell et
431 al., 2023; Wang et al., 2017), may also result in over elongation of mutant centrioles with just A-
432 tubules. In addition, we note that CPAP has an expanded domain in mutant centrioles
433 compared to controls (Fig 4 and Vásquez-Limeta et al., 2022). CPAP is involved in slow
434 processive microtubule growth (Sharma et al., 2016) and its loss results in centriole

fragmentation (Vásquez-Limeta et al., 2022), and it is possible that CPAP mislocalization may also contribute to over elongation of these mutant centrioles. Future work will determine the molecular mechanisms by which mutant centrioles lacking triplet microtubules are disassembled through the cell cycle.

Finally, we note that mutant human centrioles lacking compound microtubules bear similarities to the centrioles of *Drosophila* and *C. elegans* embryos, which have evolved to lack triplet microtubules and have cartwheels extending the entire length of the centriole (González et al., 1998; Pelletier et al., 2006; Woglar et al., 2022). Embryonic centrioles in both species are shorter than that of other organisms, and helical inner scaffolds have not been reported. In both species, these diminished centrioles participate in mitosis, can duplicate their centrioles, and serve as basal bodies for sensory cilia. We speculate that centrioles with triplet microtubules and the proteins they anchor, including the inner scaffold, may be required for centriole function in organisms with motile cilia, perhaps to help stabilize the basal body against ciliary movement. Such activity has been described for Tetrahymena basal bodies, and mutating an inner scaffold protein, Poc1, results in abnormal bending within basal bodies (Junker et al., 2022). Further supporting this hypothesis, *Drosophila* spermatocytes, one of the few cells within this species with motile cilia, have basal bodies with triplet microtubules (González et al., 1998). We note that these spermatocytes likely form triplet microtubules in an alternative manner, as *Drosophila* lacks delta-tubulin or epsilon-tubulin.

In conclusion, this work, along with our previously published study, identifies proteins required for the formation or maintenance of the centriolar triplet microtubules and maps the requirements of these proteins and the triplets in centriole architecture. Together, these results pave the way for deeper molecular understanding of the mechanisms by which the triplet microtubules are formed and maintained reproducibly within cells to form robust centrioles and cilia.

Figure legends

Figure 1. Loss of Tedc1 or Tedc2 phenocopies loss of delta-tubulin or epsilon-tubulin
(A) Immunofluorescence staining of control (RPE1 *p53*$^{-/-}$), *Tedc1*$^{-/-}$ (RPE1 *p53*$^{-/-}$; *Tedc1*$^{-/-}$), Tedc1 Rescued (RPE1 *p53*$^{-/-}$; *Tedc1*$^{-/-}$; Tedc1-Halotag-3xflag), *Tedc2*$^{-/-}$ (RPE1 *p53*$^{-/-}$; *Tedc2*$^{-/-}$), Tedc2 Rescued (RPE1 *p53*$^{-/-}$; *Tedc2*$^{-/-}$; Tedc2-V5-APEX2) cells. Top row: G1 stage cells with 2 centrioles. Bottom row: S/G2 stage cells with 4 centrioles. Blue: DAPI; Yellow: Centrin; Magenta: CP110. Images are maximum projections of confocal stacks. Scale bar: 5 um **(B)** Centriole number counts of the indicated cell lines. Cells were either asynchronous, serum-starved for G0/G1, stained for PCNA for S-phase, synchronized with RO-3306 for G2/M, or mitotic figures were identified by DAPI staining. Each condition was performed in triplicate, with n=100 cells scored for each. **(C)** Percent of centrioles in indicated cell types positive for SASS6 staining. Each condition was performed in triplicate, with n=200 cells scored for each. (D) Percent of centrioles in indicated cell types positive for CEP164 staining. Each condition was performed in triplicate, with n=100 cells scored for each. **(E)** TEM cross-section of a centriole in a G2-phase *Tedc1*$^{-/-}$ cell. **(F)** TEM cross-section of a centriole in a G2-phase *Tedc2*$^{-/-}$ cell. **(G)** Schematic of centriole formation and loss in control and *Tedc1*$^{-/-}$ or *Tedc2*$^{-/-}$ cells.

Figure 1 - Supplementary Figure 1. Genotyping of Tedc1$^{-/-}$ and Tedc2$^{-/-}$ mutant cell lines
(A) Gene structure of the Tedc1 locus in parental *p53*$^{-/-}$ cells and the *Tedc1*$^{-/-}$ mutant. Green boxes: exons; blue lines: introns; red triangles: sgRNA binding sites; black arrow: translation start site. The *Tedc1*$^{-/-}$ mutant (clone 2F4) is a compound heterozygote bearing a deletion of 227 bp on one allele and a deletion of 329 bp on the other allele. In both alleles, the ATG start site is deleted and the next ATG is not in-frame. **(B)** Gene structure of the Tedc2 locus in parental *p53*$^{-/-}$ cells and the *Tedc2*$^{-/-}$ mutant. Green boxes: exons; blue lines: introns; red triangles: sgRNA binding sites; black arrow: translation start site. The *Tedc2*$^{-/-}$ mutant (clone F5) is a compound heterozygote bearing a deletion of 19 bp on one allele flanking the ATG start site. On the other allele, there is an insertion of 306 bp corresponding to a fusion between Tedc2 and the hCLHC1 gene. In both alleles, the ATG start site is deleted, the next ATG is not in-frame, and no additional ATG start sites are found. **(C)** Genotyping PCR of the Tedc1 locus in parental *p53*$^{-/-}$ cells, the *Tedc1*$^{-/-}$ mutant, and Tedc1 Rescued (RPE1 *p53*$^{-/-}$; *Tedc1*$^{-/-}$; Tedc1-Halotag-3xflag) cells. Top: PCR for Tedc1. Bottom: PCR for Halotag. **(D)** Genotyping PCR of the Tedc2 locus in parental *p53*$^{-/-}$ cells, the *Tedc1*$^{-/-}$ mutant, and Tedc2 Rescued (RPE1 *p53*$^{-/-}$; *Tedc2*$^{-/-}$; Tedc2-V5-APEX2) cells. Top: PCR for Tedc2. Bottom: PCR for APEX2.

Figure 2. Tedc1 and Tedc2 localize to centrioles
(A) Immunofluorescence staining of Tedc1 rescue cell lines in G1, S/G2, and M. Images are maximum projections of confocal stacks. Blue: DAPI; Cyan: Centrin; Magenta: Tedc1 (localized with anti-Flag antibody); Yellow: SASS6. Scale bar: 5 um. **(B)** Immunofluorescence staining of Tedc2 rescue cell lines in G1, S/G2, and M. Images are maximum projections of confocal stacks. Blue: DAPI; Cyan: Centrin (localized with anti-GFP antibody recognizing GFP-centrin); Magenta: Tedc2 (localized with anti-V5 antibody); Yellow: SASS6. Scale bar: 5 um. **(C)** U-ExM of Tedc1 rescue cell lines, arranged by procentriole length. Cyan: Acetylated tubulin; Magenta: Tedc1 (localized with anti-Flag antibody). Confocal image stacks were deconvolved using

506 Microvolution; single plane images shown. Scale bar: 1 um. **(D)** U-ExM of Tedc2 rescue cell
507 lines, arranged by procentriole length. Cyan: Acetylated tubulin; Magenta: Tedc2 (localized with
508 anti-V5 antibody). Confocal image stacks were acquired with a Yokogawa CSU-W1 spinning
509 disk microscope and deconvolved using Microvolution; single plane images shown. Scale bar: 1
510 um.
511
512 **Figure 2 - Supplementary Figure 1. Specificity of Flag and V5 antibodies**
513 **(A)** Immunofluorescence staining of $p53^{-/-}$ cells expressing Halotag-Flag - negative control for
514 Fig 2A. Images are maximum projections of confocal stacks and were acquired with the same
515 exposure settings as in Fig 2A. Blue: DAPI; Cyan: Centrin; Magenta: Tedc1 (localized with anti-
516 Flag antibody); Yellow: SASS6. Scale bar: 5 um. **(B)** Immunofluorescence staining of $p53^{-/-}$ cells
517 expressing V5-APEX2 - negative control for Fig 2B. Images are maximum projections of
518 confocal stacks and were acquired with the same exposure settings as in Fig 2B. Blue: DAPI;
519 Cyan: Centrin (localized with anti-GFP antibody recognizing GFP-centrin); Magenta: Tedc2
520 (localized with anti-V5 antibody); Yellow: SASS6. Scale bar: 5 um. **(C)** U-ExM of $p53^{-/-}$ cells
521 expressing Halotag-Flag - negative control for Fig 2C. Cyan: Acetylated tubulin; Magenta:
522 Tedc1 (localized with anti-Flag antibody). Confocal image stacks were deconvolved using
523 Microvolution; single plane images shown. Images were acquired using the same parameters
524 as Fig 2C. Scale bar: 1 um. **(D)** U-ExM of $p53^{-/-}$ cells expressing V5-APEX2 - negative control
525 for Fig 2D. Cyan: Acetylated tubulin; Magenta: Tedc2 (localized with anti-V5 antibody). Confocal
526 image stacks were deconvolved using Microvolution; single plane images shown. Images were
527 acquired using the same parameters as Fig 2D. Scale bar: 1 um.
528
529 **Fig 2 - Supplementary Figure 2 - Tedc1 localization arranged by procentriole length and**
530 **centriole orientation**
531 U-ExM of Tedc1 rescue cell lines, arranged by procentriole length and centriole orientation.
532 Procentriole lengths are indicated in each image (um). Cyan: Acetylated tubulin; Magenta:
533 Tedc1 (localized with anti-Flag antibody). Confocal image stacks were deconvolved using
534 Microvolution; single plane images shown. Scale bar: 1 um.
535
536 **Fig 2 - Supplementary Figure 3 - Tedc2 localization arranged by procentriole length and**
537 **centriole orientation**
538 U-ExM of Tedc2 rescue cell lines, arranged by procentriole length and centriole orientation.
539 Procentriole lengths are indicated in each image (um). Cyan: Acetylated tubulin; Magenta:
540 Tedc2 (localized with anti-V5 antibody). Confocal image stacks were deconvolved using
541 Microvolution; single plane images shown. Scale bar: 1 um.
542

543 **Figure 3. Tedc1, Tedc2, TUBD1, TUBE1 form a complex in cells**
544 **(A) Centrosomal Tedc1 localization depends on Tedc2, Tubd1, Tube1.**
545 Immunofluorescence staining of cells expressing Tedc1-Halotag-3xflag. Control cell is Tedc1
546 mutant cells rescued with Tedc1-Halotag-3xflag. Images are maximum projections of confocal
547 stacks. Blue: DAPI; Cyan: SASS6; Magenta: Tedc1 (localized with anti-Flag antibody). Scale
548 bar: 5 um. **(B) Centrosomal Tedc2 localization depends on Tedc1, Tubd1, Tube1.**
549 Immunofluorescence staining of cells expressing Tedc2-V5-APEX2. Control cell is Tedc2
550 mutant cells rescued with Tedc2-V5-APEX2. Images are maximum projections of confocal
551 stacks. Blue: DAPI; Cyan: SASS6; Magenta: Tedc2 (localized with anti-V5 antibody). Scale bar:
552 5 um. **(C) Tedc1 pulls down Tedc2 in the absence of delta or epsilon-tubulin.** Western blot
553 of input and pulldown of Halotag-Flag or TEDC2-Halotag-Flag in the indicated cell lines. **(D)**
554 **Tedc2 pulls down Tedc1 in the absence of delta or epsilon-tubulin.** Western blot of input
555 and pulldown of TUBA1B-V5-APEX2 or TEDC2-V5-APEX2 in the indicated cell lines. **(E)**
556 AlphaFold Multimer prediction of the complex **(F)** AlphaFold Multimer prediction colored
557 according to pLDDT. Very high: pLDDT > 90. High: 90 > pLDDT > 70. Low: 70 > pLDDT > 50.
558 Very low: pLDDT <50 **(G)** Predicted align error of the AlphaFold Multimer prediction. Expected
559 position error (Angstroms) is graphed.
560
561 **Fig 3 - Supplementary Figure 1. AlphaFold Multimer predictions**
562 **(A)** AlphaFold Multimer prediction of TEDC1, TEDC2, TUBA1A, TUBB **(B)** AlphaFold-Multimer
563 prediction from A) colored according to pLDDT. Very high: pLDDT > 90. High: 90 > pLDDT > 70.
564 Low: 70 > pLDDT > 50. Very low: pLDDT <50 **(C)** Predicted align error of the AlphaFold-
565 Multimer prediction from A). Expected position error (Angstroms) is graphed. **(D)** AlphaFold
566 Multimer prediction of *Xenopus* TEDC1, TEDC2, TUBD1, TUBE1 **(E)** AlphaFold-Multimer
567 prediction from E) colored according to pLDDT. Very high: pLDDT > 90. High: 90 > pLDDT > 70.
568 Low: 70 > pLDDT > 50. Very low: pLDDT <50 **(F)** Predicted align error of the AlphaFold-
569 Multimer prediction from D). Expected position error (Angstroms) is graphed.
570
571 **Figure 4. Mutant centrioles elongate in G2 but fail to recruit central core proteins and**
572 **have an expanded proximal region**
573 **(A)** Lengths of expanded centrioles (um) from cells of the indicated cell cycle stages. Cells were
574 synchronized in S/G2/M and S-phase cells were marked with PCNA. The expansion factor was
575 approximately 4x (see Fig 4 - Supp fig 1). **(B)** U-ExM images of nuclei and centrioles from cells
576 of the indicated cell cycle stages and genotypes, used for quantification in A). Nuclei were
577 stained for PCNA, scale bar = 25 um. Cells in S phase had punctate PCNA staining. Centrioles
578 were stained for acetylated tubulin, scale bar = 1 um. **(C)** U-ExM of centrioles in S or G2 phase
579 stained with monoE (GT335) antibody. **(D)** U-ExM of control centrioles in S or G2 phase stained
580 with acetylated tubulin and polyE antibodies **(E) i)** U-ExM of centrioles in G2 phase stained with
581 acetylated tubulin (cyan) and POC5 (magenta) antibodies. POC5 is present in the central core
582 of control procentrioles and *de novo* centrioles, and absent from mutants. Scale bar = 1 um. **(ii)**
583 U-ExM of centrioles in G2 phase stained with acetylated tubulin (cyan) and WDR90 (magenta)
584 antibodies. WDR90 is present in the central core of control procentrioles and *de novo* centrioles,
585 and absent from mutants. Scale bar = 1 um. **(F, G, H, I)** U-ExM of centrioles in S and G2 phase
586 stained for acetylated tubulin (cyan) or monoE (GT335, cyan) and the following antibodies in

587 magenta: F) SASS6, G) CEP135, H) STIL, I) CPAP. In control centrioles, these proteins are
588 limited to the proximal end. In mutant centrioles, these proteins are present at the proximal end
589 in S phase centrioles and elongate throughout the entire centriole in G2 phase. Images were
590 acquired with a Yokogawa CSU-W1 SoRA with 2.8x relay and deconvolved with 10 iterations
591 using Microvolution. Scale bars: 1 um.
592
593 **Figure 4 - Supplementary figure 1 - Extended analyses of mutant centriole architecture**
594 **and U-ExM gel expansion factor**
595 **(A, B, C, D, E, F)** U-ExM of centrioles in S and G2 phase stained for acetylated tubulin (cyan)
596 and the following proteins in magenta: A) CEP44, B) CETN2, C) CP110, D) CEP120, E)
597 gamma-tubulin, F) CEP295. Scale bars = 1 um. Images were acquired with a Yokogawa CSU-
598 W1 SoRA with 2.8x relay and deconvolved with 10 iterations using Microvolution.
599 **(G)** Measurements of the widths of parental centrioles from each experiment as a readout of
600 expansion factor, including the cell cycle analyses in Fig 4A and Fig 4B. Centriole widths were a
601 mean of 1.0 um, corresponding to a four-fold expansion factor.
602
603 **Figure 4 - Supplementary figure 2 - Total protein levels of centrosomal proteins are**
604 **unchanged in mutant cells**
605 **(A)** Western blot of control (RPE1 *p53*$^{-/-}$), *Tedc1*$^{-/-}$, *Tedc2*$^{-/-}$, *Tubd1*$^{-/-}$, *Tube1*$^{-/-}$, *Sas6*$^{-/-}$ cell
606 lysates, immunoblotted for SAS6. Total protein stain (Revert) serves as a loading control. **(B)**
607 Western blot of control (RPE1 *p53*$^{-/-}$), *Tedc1*$^{-/-}$, *Tedc2*$^{-/-}$, *Tubd1*$^{-/-}$, *Tube1*$^{-/-}$ cell lysates,
608 immunoblotted for STIL. Total protein stain (Revert) serves as a loading control. **(C)** Western
609 blot of control (RPE1 *p53*$^{-/-}$), *Tedc1*$^{-/-}$, *Tedc2*$^{-/-}$, *Tubd1*$^{-/-}$, *Tube1*$^{-/-}$ cell lysates, immunoblotted for
610 CPAP. Total protein stain (Revert) serves as a loading control. **(D)** Western blot of control
611 (RPE1 *p53*$^{-/-}$), *Tedc1*$^{-/-}$, *Tedc2*$^{-/-}$, *Tubd1*$^{-/-}$, *Tube1*$^{-/-}$ cell lysates, immunoblotted for POC5. Total
612 protein stain (Revert) serves as a loading control.
613
614 **Fig 5. Mutant centrioles elongate further in mitosis before fragmenting**
615 U-ExM of centrioles stained for monoE (GT335, cyan), CP110 (yellow) and SASS6 (magenta).
616 **(A)** A prometaphase cell with centrioles formed *de novo* **(B)** An anaphase cell with centrioles
617 formed *de novo* **(C)** A prometaphase *Tubd1*$^{-/-}$ cell **(D)** A telophase *Tubd1*$^{-/-}$ cell **(E)** A
618 prometaphase *Tube1*$^{-/-}$ cell **(F)** An anaphase *Tube1*$^{-/-}$ cell. Scale bars: 1 um. Images were
619 acquired with a Yokogawa CSU-W1 SoRA with 2.8x relay.
620

621 ## Materials and Methods
622
623 **Cell lines and cell culture**
624 hTERT RPE-1 *TP53*$^{-/-}$ cells were a gift from Meng-Fu Bryan Tsou (Memorial Sloan Kettering
625 Cancer Center) and were cultured in DMEM/F-12 (Corning) supplemented with 10% Cosmic
626 Calf Serum (CCS; HyClone). HEK293T cells for lentivirus production (see below) were obtained
627 from the ATCC and cultured in DMEM (Corning) supplemented with 10% CCS. hTERT RPE-1
628 and HEK293T/17 cells were authenticated using STR profiling using CODIS loci. All other cell
629 lines used were derived from hTERT RPE-1 *TP53*$^{-/-}$ cells. Stable *Tp53*$^{-/-}$*; Tedc1*$^{-/-}$ and *Tp53*$^{-/-}$*;*
630 *Tedc2*$^{-/-}$ knockout cell lines were made in the hTERT RPE-1 *Tp53*$^{-/-}$ cells by CRISPR/Cas9
631 (see below). For rescue experiments, clonal knockout cell lines were rescued using lentiviral
632 transduction (see below). All cells were cultured at 37°C under 5% CO_2, and are mycoplasma-
633 free (Uphoff and Drexler, 2011).
634
635 **Generation of *Tedc1*$^{-/-}$ and *Tedc2*$^{-/-}$ cells and rescue cell lines**
636 *Tedc1*$^{-/-}$ and *Tedc2*$^{-/-}$ cells were generated by CRISPR/Cas9 mediated gene editing using a
637 recombinantly produced, purified Cas9 protein (Cas9-NLS, QB3 Macrolab, Berkeley) and
638 chemically synthetized two-component gRNA (crRNA:tracrRNA, Alt-R CRISPR-Cas9 system,
639 IDT). For increased efficiency, two gRNAs, both targeting the 5' end of each gene, were used at
640 the same time. Target sequences were: 5'-CGCCAAGTTCGACCGTCCGG-3' and 5'-
641 CGTCCAATCACCGCACGGGC-3' for TEDC1, and 5'-CGCACAGCGACAATTGCAAT-3' and 5'-
642 CACCGGCGCGAGCAGCCCGC-3' for TEDC2.
643
644 Lyophilized RNA oligos were reconstituted according to the instructions provided by the
645 manufacturer (IDT). Briefly, oligos were reconstituted in the duplex buffer at a concentration of
646 200 µM. To anneal crRNA with tracrRNA, 3 µl of each (600 pmol) were mixed, heated to 95°C,
647 and transferred to room temperature to gradually cool. Pre-complexed crRNA and tracrRNA
648 (550 pmol) were mixed with purified Cas9 (360 pmol), diluted with PBS to a total volume of 25 µl
649 and incubated for 15 min at room temperature to form ribonucloprotein complexes (RNPs).
650
651 RPE1 *Tp53*$^{-/-}$ cells stably expressing GFP-centrin (Wang et al., 2017) were electroporated in a
652 home-made electroporation buffer (Zhang et al., 2014) using Amaxa Nucleofector II (Lonza).
653 Cells were electroporated with an equal mix of two RNPs: 50 µl of RNPs mixture was added to 2
654 x 10^6 cells in 200 µl electroporation buffer. To facilitate the identification of electroporated cells,
655 an mRuby2 expressing plasmid (pcDNA3-mRuby2, plasmid pTS3994) was electroporated
656 together with RNPs.
657
658 Two days after electroporation, cells expressing mRuby2 were sorted using FACS, and single
659 cells were plated into 96 well plates in conditioned media. Surviving clones were genotyped by
660 PCR of genomic DNA and screened for phenotype based on centrin-GFP expression.
661

662 Primers used for genotyping were: 5'CCCTGCCGACGCAGTGATTGG3' and
663 5'CAGGGAGTGGCGAGAGCACAC3' for TEDC1 and 5' CTTGCCCGCAAGGAGGGAGAGA3'
664 and 5'GCAGGGCCCAGCCCAAACAGA3' for TEDC2.
665
666 To rescue the mutations, Halo-3xFlag-tagged TEDC1 or APEX-V5-tagged TEDC2 were
667 introduced into the mutant cells using lentiviral transduction as described below.
668
669 **Lentivirus production and viral transduction**
670 Recombinant lentiviruses were made by cotransfection of HEK293T cells with the respective
671 transfer vectors (TEDC1-Halotag-3xFlag and TEDC2-V5-APEX2), second-generation lentiviral
672 cassettes (packaging vector psPAX2, pTS3312 and envelope vector pMD2.G, pTS3313) using
673 calcium phosphate-mediated transfection. Briefly, transfection mixture was made with CaCl2, 2x
674 HBS (50 mM Hepes, 10 mM KCl, 12 mM dextrose, 280 mM NaCl, 1.5 mM Na2HPO4x7H2O, pH
675 7.05), and plasmids. Cells were treated with 25 uM chloroquine immediately before transfection,
676 then the transfection mixture was added to cells. The medium was changed 5-6 h after
677 transfection, and viral supernatant was harvested after an additional 48 and 72 h. Recipient
678 cells (RPE-1 *Tp53*$^{-/-}$*; Tedc1*$^{-/-}$ and *Tp53*$^{-/-}$*; Tedc2*$^{-/-}$ and *Tp53*$^{-/-}$*; Tubd1*$^{-/-}$ and *Tp53*$^{-/-}$*;*
679 *Tube1*$^{-/-}$) were transduced with viral supernatant and 8 ug/mL Sequabrene. Transduced cells
680 were expanded to 10-cm dishes.
681
682 **Immunofluorescence**
683 Cells were grown on poly-L-lysine-coated #1.5 glass coverslips (Electron Microscopy Sciences).
684 Cells were fixed with −20°C methanol for 15 min. Coverslips were then washed with PBS for 10
685 min and blocked with PBS-BT (3% BSA, 0.1% Triton X-100, 0.02% sodium azide in PBS) for 30
686 min. Coverslips were incubated with primary antibodies diluted in PBS-BT for 1 hr, washed with
687 PBS-BT, incubated with secondary antibodies and DAPI diluted in PBS-BT for 1 hr, then
688 washed again. Samples were mounted using Mowiol (Polysciences) in glycerol containing 1,4,-
689 diazobicycli-[2.2.2]octane (DABCO, Sigma-Aldrich) antifade.
690
691 **Cell cycle synchronization**
692 For cell cycle analyses in Fig 1, cells were seeded onto coverslips, then synchronized in G0/G1
693 by serum withdrawal for 24 hr, or in G2 with 10 μM RO-3306 (Adipogen) for 24 hr. Cells were
694 fixed for immunofluorescence and analyzed for centrin/CP110 presence.

695 For Fig 4 and 5, mitotic shakeoff was performed on asynchronously growing cells. One pre-
696 shake was performed to improve synchronization. Cells were fixed for U-ExM and expanded as
697 below.

698 **Ultrastructure expansion microscopy (U-ExM)**

699 Cells were grown on poly-D-lysine-coated #1.5 glass coverslips (Electron Microscopy Sciences)
700 and fixed with −20°C methanol for 15 min, then washed with PBS. U-ExM was performed as
701 previously described (Gambarotto et al., 2019): coverslips were incubated overnight in an
702 acrylamide–formaldehyde anchoring solution (AA/FA; 0.7% formaldehyde, 1% acrylamide in
703 PBS) at 37°C. Gelation was allowed to proceed in monomer solution (19% sodium acrylate,
704 10% acrylamide, 0.1% bis-acrylamide, 0.5% ammonium persulfate-APS, 0.5% TEMED) for 1
705 hour at 37°C. Gels were heated in denaturation buffer (200 mM SDS, 200 mM NaCl, 50 mM
706 Tris-HCl pH 9) at 95°C for 1 h. After denaturation buffer was removed, gels were washed with
707 multiple water rinses and allowed to expand in water at room temperature overnight. Small
708 circles of each expanded gel (~5 mm in diameter) were excised and incubated with primary
709 antibodies diluted in PBS-BT (3% BSA, 0.1% Triton X-100 in PBS) on a nutator at 4°C
710 overnight. (Exception: the WDR90 antibody was incubated at 37°C overnight, as reported in
711 Steib et al., 2020). The next day, gels were washed three times with PBS-BT buffer and
712 incubated with secondary antibodies and 5 µg/ml DAPI diluted in PBS-BT, protected from light,
713 on a nutator at 4°C overnight. Immunostained gels were washed once with PBS and at least
714 three times with water, and placed in a glass-bottomed 35 mm plate for imaging. All U-ExM
715 images were acquired as *z*-stacks collected at 0.27-µm intervals using a confocal Zeiss Axio
716 Observer microscope (Carl Zeiss) with a PlanApoChromat 1.4 NA 63× oil immersion objective, a
717 Yokogawa CSU-W1 (Fig 2) or Yokogawa CSU-W1 SoRA head with 2.8x relay (Fig 4, 5) and a
718 Photometrics Prime BSI express CMOS camera. Slidebook software (Intelligent Imaging
719 Innovations, 3i) was used to control the microscope system. Deconvolution was performed with
720 Microvolution (Cupertino, CA) using a calculated point spread function (PSF) for 10 iterations.
721 ImageJ (FIJI) was used for image analysis (Schindelin et al., 2012). For measuring centriole
722 width or length, z-stacks of U-ExM images were measured using ImageJ (FIJI) on maximum
723 projections. Only centrioles that were in perfect longitudinal or cross-section were measured.
724 Three measurements were made per centriole and averaged.
725

726 **Transmission electron microscopy.** For ultrastructural analysis of centrosomes by TEM,
727 RPE-1 *p53*$^{-/-}$ *; Tedc1*$^{-/-}$ and RPE-1 *p53*$^{-/-}$ *; Tedc2*$^{-/-}$ cells were synchronized in G2/M with 10 uM
728 RO-3306 for 24 hrs. Cells were trypsinized, resuspended in complete media and centrifuged at
729 800g for 5 min. The pellet was collected in a 14-mL tube and fixed in 2%
730 paraformaldehyde/2.5% glutaraldehyde (Ted Pella Inc., Redding, CA) in 100 mM cacodylate
731 buffer, pH 7.2 for 2 hr at room temperature. Samples were washed in cacodylate buffer and
732 postfixed in 1% osmium tetroxide (Ted Pella Inc.)/1.5% potassium ferricyanide (Sigma, St.
733 Louis, MO) for 1 hr. Samples were then rinsed extensively in dH_2O prior to en bloc staining with
734 1% aqueous uranyl acetate (Ted Pella Inc.) for 1 hr. Following several rinses in dH_2O, samples
735 were dehydrated in a graded series of ethanol and embedded in Eponate 12 resin (Ted Pella
736 Inc.). Ultrathin sections of 95 nm were cut with a Leica Ultracut UCT ultramicrotome (Leica
737 Microsystems Inc., Bannockburn, IL), stained with uranyl acetate and lead citrate, and viewed
738 on a JEOL 1200 EX transmission electron microscope (JEOL USA Inc., Peabody, MA)
739 equipped with an AMT 8 megapixel digital camera and AMT Image Capture Engine V602
740 software (Advanced Microscopy Techniques, Woburn, MA).
741
742 **TEDC1 and TEDC2 pulldowns**
743 Cells stably expressing TEDC1-Halotag-3xFlag or TEDC2-V5-APEX2 were lysed in 50 mM Tris
744 pH7.5, 150 mM NaCl, 1% Triton X-100, 1 mM DTT, Halt protease and phosphatase inhibitor
745 cocktail (ThermoFisher Scientific) for 30 minutes on ice, then cleared by centrifugation at 21,000
746 g for 20 min. Protein concentration was determined by Pierce BCA Protein Assay - Reducing
747 Agent Compatible (ThermoFisher Scientific). Each cell lysate was incubated with 25 uL of
748 equilibrated Chromotek Halo-Trap Magnetic Agarose (Proteintech) or Chromotek V5-Trap
749 Magnetic Agarose (Proteintech) for 1 h at 4C on a nutator. Beads were washed using a
750 magnetic separator rack. Elution was performed by adding 80 uL of 2x SDS loading buffer (100
751 mM Tris pH 6.8, 4% SDS, 20% glycerol, 100 mM DTT), boiling the beads for 5 min at 95C, then
752 separating the eluate with a magnetic separator rack. Samples were loaded on SDS-PAGE and
753 transferred for Western blotting.
754
755 **Western blotting**
756 For Fig 4 - Supp 2, samples were lysed in 50 mM Tris pH7.5, 150 mM NaCl, 1% Triton X-100, 1
757 mM DTT, Halt protease and phosphatase inhibitor cocktail (ThermoFisher Scientific) for 30
758 minutes on ice, then cleared by centrifugation at 21,000 g for 20 min. Protein concentration was
759 determined by Pierce BCA Protein Assay - Reducing Agent Compatible (ThermoFisher
760 Scientific). Equal amounts of protein (20 to 40 ug) was loaded per lane. For Fig 3, samples were
761 loaded after pulldowns.
762
763 Proteins were separated by SDS-PAGE and transferred to nitrocellulose (LiCOR Biosciences) in
764 transfer buffer (192 mM Glycine, 25 mM Tris, 20% ethanol). Membranes were blocked with 5%
765 milk in TBST (137 mM NaCl, 25 mM Tris, 2.7 mM KCl, 0.1% Tween-20) at room temp for 1 h,
766 then washed three times with TBST for 5 min each wash. Membranes were incubated with
767 primary antibodies overnight at 4C on a nutator. The next day, membranes were washed three
768 times with TBST for 5 min each wash and incubated with secondary antibodies at room
769 temperature for 2.5 hours. Membranes were washed again with TBST for 5 min each wash and

770 then imaged with the LiCOR Odyssey XF imager and analyzed using Image Studio (LiCOR
771 Biosciences). Each experiment was performed in triplicate.
772
773 **Antibodies**
774 Primary antibodies used for immunofluorescence and U-ExM and dilutions in PBS-BT: mouse
775 IgG2b anti-acetylated-tubulin, clone 6-11B-1 (1:1000,Sigma-Aldrich Cat# T6793,
776 RRID:AB_477585), rabbit anti-acetyl-α-tubulin (Lys40) (1:100, Cell Signaling Technology Cat#
777 5335, RRID:AB_10544694), mouse IgG2b anti-centrin3, clone 3e6 (1:1000, Novus Biological,
778 RRID:AB_537701), mouse IgG2a anti-centrin, clone 20H5 (IF 1:200, UExM 1:500, EMD
779 Millipore, RRID:AB_10563501), rat anti-Cep120 (1:1000, gift from Moe Mahjoub (Betleja et al.,
780 2018)), rabbit anti-Cep135 (1:500, Proteintech Cat# 24428-1-AP, RRID:AB_2879543), rabbit
781 anti-Cep295 (1:1000, Sigma-Aldrich Cat# HPA038596, RRID:AB_10672720), rabbit anti-Cep44
782 (1:100, Proteintech Cat# 24457-1-AP, RRID:AB_2879557), rabbit anti-CENPJ (1:500,
783 Proteintech Cat# 11517-1-AP, RRID:AB_2244605), rabbit anti-CP110 (IF 1:200, UExM 1:2000,
784 Proteintech Cat# 12780-1-AP, RRID:AB_10638480), mouse IgG1 anti-Flag, clone M2 (1:500,
785 Sigma-Aldrich Cat# F1804, RRID:AB_262044), mouse IgG1 anti-gamma-tubulin, clone GTU-88
786 (IF 1:1000, UExM 1:500, Sigma-Aldrich, RRID:AB_477584), mouse IgG2a anti-PCNA (1:500,
787 BioLegend, RRID:AB_314692), rabbit anti-POC5 (for IF: 1:500, Bethyl Laboratories,
788 RRID:AB_10949152), rabbit anti-POC5 (for U-ExM: 1:500, Thermo Fisher Scientific Cat# A303-
789 341A (also A303-341A-T), RRID:AB_10971172), mouse IgG1 anti-polyglutamylation, clone
790 GT335 (1:500, AdipoGen Cat# AG-20B-0020, RRID:AB_2490210), rabbit anti-polyglutamate-
791 chain, polyE (1:500, AdipoGen Cat# AG-25B-0030, RRID:AB_2490540), mouse IgG2b anti-
792 SASS6 (1:200, Santa Cruz Cat# sc-81431, RRID:AB_1128357), rabbit anti-STIL (1:500, Abcam
793 Cat# ab89314, RRID:AB_2197878), mouse IgG2a anti-V5 (1:00, Thermo Fisher Scientific Cat#
794 R960-25, RRID:AB_2556564), rabbit anti-WDR90 (1:100, Thermo Fisher Scientific Cat# PA5-
795 61943, RRID:AB_2649628).
796
797 For immunofluorescence and U-ExM, AlexaFluor conjugated secondary antibodies (Thermo-
798 Fisher) were diluted 1:1000 in PBS-BT. Goat anti-Mouse IgG1, 488 (1:1000, Thermo Fisher
799 Scientific Cat# A-21121, RRID:AB_2535764), Goat anti-Mouse IgG2a, 488 (1:1000, Thermo
800 Fisher Scientific Cat# A-21131, RRID:AB_2535771), Goat anti-Mouse IgG2b, 488 (1:1000,
801 Thermo Fisher Scientific Cat# A-21141, RRID:AB_2535778), Goat anti-rabbit IgG (H+L), 488
802 (1:1000, Thermo Fisher Scientific Cat# A-11034 (also A11034), RRID:AB_2576217), Goat anti-
803 Mouse IgG1, 568 (1:500, Thermo Fisher Scientific Cat# A-21124, RRID:AB_2535766), Goat
804 anti-Mouse IgG2a, 568 (1:500, Thermo Fisher Scientific Cat# A-21134, RRID:AB_2535773),
805 Goat anti-Mouse IgG2b, 568 (1:500, Thermo Fisher Scientific Cat# A-21144,
806 RRID:AB_2535780), Goat anti-rabbit IgG (H+L), 568 (1:500, Thermo Fisher Scientific Cat# A-
807 11036 (also A11036), RRID:AB_10563566), Goat anti-Mouse IgG3, 594 (1:500, Thermo Fisher
808 Scientific Cat# A-21155, RRID:AB_2535785), Goat anti-rat IgG (H+L), 594 (1:500,Thermo
809 Fisher Scientific Cat# A-11007 (also A11007), RRID:AB_10561522), Goat anti-Mouse IgG1,
810 647 (1:500, Thermo Fisher Scientific Cat# A-21240, RRID:AB_2535809), Goat anti-Mouse
811 IgG2a, 647 (1:500, Thermo Fisher Scientific Cat# A-21241, RRID:AB_2535810), Goat anti-
812 Mouse IgG2b, 647 (1:500, Thermo Fisher Scientific Cat# A-21242, RRID:AB_2535811), Goat
813 anti-rabbit IgG (H+L), 647 (1:500, Thermo Fisher Scientific Cat# A32733, RRID:AB_2633282)

Primary antibodies used for Western blotting and dilutions in TBST: rabbit anti TUBD1 (1:1000, Sigma-Aldrich Cat# HPA027090, RRID:AB_1858457), rabbit anti TUBE1 (1:1000, Sigma-Aldrich Cat # HPA032074, RRID:AB_10601216), rabbit anti C14orf80 (1:1000, Sigma-Aldrich Cat # HPA039049, RRID:AB_2676320), rabbit anti C16orf59 (1:1000, Sigma-Aldrich Cat # HPA055389, RRID:AB_2732595), mouse IgG2b anti SASS6 (1:200, Santa Cruz Biotech Cat # sc-81431, RRID:AB_1128357), rabbit anti STIL (1:2000, Abcam Cat# ab89314, RRID:AB_2197878), rabbit anti CENPJ/CPAP (1:1000, Proteintech Cat# 11517-1-AP, RRID:AB_2244605), rabbit anti POC5 (1:1000, Thermo Fisher Scientific Cat# A303-341A (also A303-341A-T), RRID:AB_10971172), mouse IgG2a anti V5 (1:1000, Thermo Fisher Scientific Cat# R960-25, RRID:AB_2556564), mouse IgG1 anti Flag, clone M2 (1:2000, Sigma-Aldrich Cat# F1804, RRID:AB_262044). Secondary antibodies used for Western blotting: 680 Donkey anti rabbit (H+L) (1:20,000, Thermo Fisher Scientific Cat# A10043, RRID:AB_2534018), 800 Donkey anti rabbit (H+L) (1:20,000, Li-COR Cat# 926-32213, RRID:AB_621848), 680 Donkey anti mouse (H+L) (1:20,000, Thermo Fisher Scientific Cat# A10038, RRID:AB_11180593), 800 Donkey anti mouse (H+L) (1:20,000, Li-COR Cat# 926-32212, RRID:AB_621847).

Acknowlegments

This work was supported by NIH/NIGMS (K99/R00 GM131024 to J.T.W. and R35 GM130286 to T.S.) and Washington University startup funds (to J.T.W). We thank Wandy Beatty of the Washington University Molecular Microbiology Imaging Facility for assistance with transmission electron microscopy, Moe Mahjoub (Washington University School of Medicine) for the gift of the CEP120 and goat anti-rat antibodies and Meng-Fu Bryan Tsou (Memorial Sloan Kettering Cancer Center) for the gifts of RPE-1 *p53*$^{-/-}$ and RPE-1 *p53*$^{-/-}$ *; SAS6*$^{-/-}$ cells. We thank the Stanford cytoskeleton group, WashU centrosome/cilia group, members of the Stearns lab, and David Breslow for helpful discussions. We also thank Hani Zaher's and Joe Jez's labs for hosting the Wang lab during renovations and Larry Galloway for help with Python.

References

Arslanhan, M. D., Cengiz-Emek, S., Odabasi, E., Steib, E., Hamel, V., Guichard, P. and Firat-Karalar, E. N. (2023). CCDC15 localizes to the centriole inner scaffold and controls centriole length and integrity. *Journal of Cell Biology* **222**, e202305009.

Betleja, E., Nanjundappa, R., Cheng, T. and Mahjoub, M. R. (2018). A novel Cep120-dependent mechanism inhibits centriole maturation in quiescent cells. *eLife* **7**, e35439.

Breslow, D. K. and Holland, A. J. (2019). Mechanism and Regulation of Centriole and Cilium Biogenesis. *Annu. Rev. Biochem.* **88**, 691–724.

Breslow, D. K., Hoogendoorn, S., Kopp, A. R., Morgens, D. W., Vu, B. K., Kennedy, M. C., Han, K., Li, A., Hess, G. T., Bassik, M. C., et al. (2018). A CRISPR-based screen for Hedgehog signaling provides insights into ciliary function and ciliopathies. *Nat Genet* **50**, 460–471.

Comartin, D., Gupta, G. D., Fussner, E., Coyaud, É., Hasegan, M., Archinti, M., Cheung, S. W. T., Pinchev, D., Lawo, S., Raught, B., et al. (2013). CEP120 and SPICE1 Cooperate with CPAP in Centriole Elongation. *Current Biology* **23**, 1360–1366.

de Loubresse, N. G., Ruiz, F. and Beisson, J. (2001). Role of delta-tubulin and the C-tubule in assembly of Paramecium basal bodies. *BMC Cell Biology* 7.

Dupuis-Williams, P., Fleury-Aubusson, A., de Loubresse, N. G., Geoffroy, H., Vayssié, L., Galvani, A., Espigat, A. and Rossier, J. (2002). Functional role of ε-tubulin in the assembly of the centriolar microtubule scaffold. *Journal of Cell Biology* **158**, 1183–1193.

Dutcher, S. K. and Trabuco, E. C. (1998). The UNI3 Gene Is Required for Assembly of Basal Bodies of Chlamydomonas and Encodes ʕ-Tubulin, a New Member of the Tubulin Superfamily. *Molecular Biology of the Cell* **9**, 16.

Dutcher, S. K., Morrissette, N. S., Preble, A. M., Rackley, C. and Stanga, J. (2002). ᔑ-Tubulin Is an Essential Component of the Centriole. *Molecular Biology of the Cell* **13**, 11.

Evans, R., O'Neill, M., Pritzel, A., Antropova, N., Senior, A., Green, T., Žídek, A., Bates, R., Blackwell, S., Yim, J., et al. (2021). *Protein complex prediction with AlphaFold-Multimer*. Bioinformatics.

Farrell, K., Wang, J. T. and Stearns, T. (2023). *Spindle assembly checkpoint-dependent mitotic delay is required for cell division in absence of centrosomes*. elife.

Gadelha, C., Wickstead, B., McKean, P. G. and Gull, K. (2006). Basal body and flagellum mutants reveal a rotational constraint of the central pair microtubules in the axonemes of trypanosomes. *Journal of Cell Science* **119**, 2405–2413.

Gambarotto, D., Zwettler, F. U., Le Guennec, M., Schmidt-Cernohorska, M., Fortun, D., Borgers, S., Heine, J., Schloetel, J.-G., Reuss, M., Unser, M., et al. (2019). Imaging cellular ultrastructures using expansion microscopy (U-ExM). *Nat Methods* **16**, 71–74.

González, C., Tavosanis, G. and Mollinari, C. (1998). Centrosomes and microtubule organisation during *Drosophila* development. *Journal of Cell Science* **111**, 2697–2706.

Goodenough, U. W. and StClair, H. S. (1975). BALD-2: a mutation affecting the formation of doublet and triplet sets of microtubules in Chlamydomonas reinhardtii. *Journal of Cell Biology* **66**, 480–491.

Guichard, P. and Gönczy, P. (2016). Basal body structure in Trichonympha. *Cilia* **5**, 9.

Guichard, P., Desfosses, A., Maheshwari, A., Hachet, V., Dietrich, C., Brune, A., Ishikawa, T., Sachse, C. and Gönczy, P. (2012). Cartwheel Architecture of *Trichonympha* Basal Body. *Science* **337**, 553–553.

Guichard, P., Laporte, M. H. and Hamel, V. (2023). The centriolar tubulin code. *Seminars in*

Cell & Developmental Biology **137**, 16–25.
Hatzopoulos, G. N., Erat, M. C., Cutts, E., Rogala, K. B., Slater, L. M., Stansfeld, P. J. and Vakonakis, I. (2013). Structural Analysis of the G-Box Domain of the Microcephaly Protein CPAP Suggests a Role in Centriole Architecture. *Structure* **21**, 2069–2077.
Hilbert, M., Noga, A., Frey, D., Hamel, V., Guichard, P., Kraatz, S. H. W., Pfreundschuh, M., Hosner, S., Flückiger, I., Jaussi, R., et al. (2016). SAS-6 engineering reveals interdependence between cartwheel and microtubules in determining centriole architecture. *Nat Cell Biol* **18**, 393–403.
Huttlin, E. L., Bruckner, R. J., Paulo, J. A., Cannon, J. R., Ting, L., Baltier, K., Colby, G., Gebreab, F., Gygi, M. P., Parzen, H., et al. (2017). Architecture of the human interactome defines protein communities and disease networks. *Nature* **545**, 505–509.
Huttlin, E. L., Bruckner, R. J., Navarrete-Perea, J., Cannon, J. R., Baltier, K., Gebreab, F., Gygi, M. P., Thornock, A., Zarraga, G., Tam, S., et al. (2021). Dual proteome-scale networks reveal cell-specific remodeling of the human interactome. *Cell* **184**, 3022-3040.e28.
Izquierdo, D., Wang, W.-J., Uryu, K. and Tsou, M.-F. B. (2014). Stabilization of Cartwheel-less Centrioles for Duplication Requires CEP295-Mediated Centriole-to-Centrosome Conversion. *Cell Reports* **8**, 957–965.
Junker, A. D., Woodhams, L. G., Soh, A. W. J., O'Toole, E. T., Bayly, P. V. and Pearson, C. G. (2022). Basal bodies bend in response to ciliary forces. *MBoC* **33**, ar146.
Kann, M., Soues, S., Levilliers, N. and Fouquet, J. (2003). Glutamylated tubulin: Diversity of expression and distribution of isoforms. *Cell Motil. Cytoskeleton* **55**, 14–25.
Klena, N., Le Guennec, M., Tassin, A., Van Den Hoek, H., Erdmann, P. S., Schaffer, M., Geimer, S., Aeschlimann, G., Kovacik, L., Sadian, Y., et al. (2020). Architecture of the centriole cartwheel-containing region revealed by cryo-electron tomography. *The EMBO Journal* **39**, e106246.
Kleylein-Sohn, J., Westendorf, J., Le Clech, M., Habedanck, R., Stierhof, Y.-D. and Nigg, E. A. (2007). Plk4-Induced Centriole Biogenesis in Human Cells. *Developmental Cell* **13**, 190–202.
Kong, D., Sahabandu, N., Sullenberger, C., Vásquez-Limeta, A., Luvsanjav, D., Lukasik, K. and Loncarek, J. (2020). Prolonged mitosis results in structurally aberrant and over-elongated centrioles. *Journal of Cell Biology* **219**, e201910019.
Kraatz, S., Guichard, P., Obbineni, J. M., Olieric, N., Hatzopoulos, G. N., Hilbert, M., Sen, I., Missimer, J., Gönczy, P. and Steinmetz, M. O. (2016). The Human Centriolar Protein CEP135 Contains a Two-Stranded Coiled-Coil Domain Critical for Microtubule Binding. *Structure* **24**, 1358–1371.
Kumar, D., Rains, A., Herranz-Pérez, V., Lu, Q., Shi, X., Swaney, D. L., Stevenson, E., Krogan, N. J., Huang, B., Westlake, C., et al. (2021). A ciliopathy complex builds distal appendages to initiate ciliogenesis. *Journal of Cell Biology* **220**, e202011133.
Laporte, M. H., Bouhlel, I. B., Bertiaux, E., Morrison, C. G., Giroud, A., Borgers, S., Azimzadeh, J., Bornens, M., Guichard, P., Paoletti, A., et al. (2022). Human SFI1 and Centrin form a complex critical for centriole architecture and ciliogenesis. *The EMBO Journal* **41**, e112107.
Le Borgne, P., Greibill, L., Laporte, M. H., Lemullois, M., Bouhouche, K., Temagoult, M., Rosnet, O., Le Guennec, M., Lignières, L., Chevreux, G., et al. (2022). The evolutionary conserved proteins CEP90, FOPNL, and OFD1 recruit centriolar distal appendage proteins to initiate their assembly. *PLoS Biol* **20**, e3001782.
Le Guennec, M., Klena, N., Gambarotto, D., Laporte, M. H., Tassin, A.-M., Van Den Hoek, H., Erdmann, P. S., Schaffer, M., Kovacik, L., Borgers, S., et al. (2020). A helical inner scaffold provides a structural basis for centriole cohesion. *Sci. Adv.* **6**, eaaz4137.
LeGuennec, M., Klena, N., Aeschlimann, G., Hamel, V. and Guichard, P. (2021). Overview

of the centriole architecture. *Current Opinion in Structural Biology* **66**, 58–65.
Lin, Y.-C., Chang, C.-W., Hsu, W.-B., Tang, C.-J. C., Lin, Y.-N., Chou, E.-J., Wu, C.-T. and Tang, T. K. (2013a). Human microcephaly protein CEP135 binds to hSAS-6 and CPAP, and is required for centriole assembly. *EMBO J* **32**, 1141–1154.
Lin, Y.-N., Wu, C.-T., Lin, Y.-C., Hsu, W.-B., Tang, C.-J. C., Chang, C.-W. and Tang, T. K. (2013b). CEP120 interacts with CPAP and positively regulates centriole elongation. *Journal of Cell Biology* **202**, 211–219.
Mahecic, D., Gambarotto, D., Douglass, K. M., Fortun, D., Banterle, N., Ibrahim, K. A., Le Guennec, M., Gönczy, P., Hamel, V., Guichard, P., et al. (2020). Homogeneous multifocal excitation for high-throughput super-resolution imaging. *Nat Methods* **17**, 726–733.
Mahjoub, M. R., Xie, Z. and Stearns, T. (2010). Cep120 is asymmetrically localized to the daughter centriole and is essential for centriole assembly. *Journal of Cell Biology* **191**, 331–346.
Pelletier, L., O'Toole, E., Schwager, A., Hyman, A. A. and Müller-Reichert, T. (2006). Centriole assembly in Caenorhabditis elegans. *Nature* **444**, 619–623.
Pierron, M., Woglar, A., Busso, C., Jha, K., Mikeladze-Dvali, T., Croisier, M. and Gönczy, P. (2023). Centriole elimination during *Caenorhabditis elegans* oogenesis initiates with loss of the central tube protein SAS -1. *The EMBO Journal* **42**, e115076.
Pimenta-Marques, A., Bento, I., Lopes, C. a. M., Duarte, P., Jana, S. C. and Bettencourt-Dias, M. (2016). A mechanism for the elimination of the female gamete centrosome in Drosophila melanogaster. *Science* **353**, aaf4866.
Ross, I., Clarissa, C., Giddings, T. H. and Winey, M. (2013). ε-tubulin is essential in *Tetrahymena thermophila* for the assembly and stability of basal bodies. *Journal of Cell Science* jcs.128694.
Sahabandu, N., Kong, D., Magidson, V., Nanjundappa, R., Sullenberger, C., Mahjoub, M. R. and Loncarek, J. (2019). Expansion microscopy for the analysis of centrioles and cilia. *Journal of Microscopy* **276**, 145–159.
Schindelin, J., Arganda-Carreras, I., Frise, E., Kaynig, V., Longair, M., Pietzsch, T., Preibisch, S., Rueden, C., Saalfeld, S., Schmid, B., et al. (2012). Fiji: an open-source platform for biological-image analysis. *Nat Methods* **9**, 676–682.
Schweizer, N., Haren, L., Dutto, I., Viais, R., Lacasa, C., Merdes, A. and Lüders, J. (2021). Sub-centrosomal mapping identifies augmin-γTuRC as part of a centriole-stabilizing scaffold. *Nat Commun* **12**, 6042.
Sharma, A., Aher, A., Dynes, N. J., Frey, D., Katrukha, E. A., Jaussi, R., Grigoriev, I., Croisier, M., Kammerer, R. A., Akhmanova, A., et al. (2016). Centriolar CPAP/SAS-4 Imparts Slow Processive Microtubule Growth. *Developmental Cell* **37**, 362–376.
Spektor, A., Tsang, W. Y., Khoo, D. and Dynlacht, B. D. (2007). Cep97 and CP110 Suppress a Cilia Assembly Program. *Cell* **130**, 678–690.
Steib, E., Laporte, M. H., Gambarotto, D., Olieric, N., Zheng, C., Borgers, S., Olieric, V., Le Guennec, M., Koll, F., Tassin, A.-M., et al. (2020). WDR90 is a centriolar microtubule wall protein important for centriole architecture integrity. *eLife* **9**, e57205.
Uphoff, C. C. and Drexler, H. G. (2011). Detecting Mycoplasma Contamination in Cell Cultures by Polymerase Chain Reaction. In *Cancer Cell Culture* (ed. Cree, I. A.), pp. 93–103. Totowa, NJ: Humana Press.
Van Dijk, J., Rogowski, K., Miro, J., Lacroix, B., Eddé, B. and Janke, C. (2007). A Targeted Multienzyme Mechanism for Selective Microtubule Polyglutamylation. *Molecular Cell* **26**, 437–448.
Vásquez-Limeta, A., Lukasik, K., Kong, D., Sullenberger, C., Luvsanjav, D., Sahabandu, N., Chari, R. and Loncarek, J. (2022). CPAP insufficiency leads to incomplete centrioles that duplicate but fragment. *Journal of Cell Biology* **221**, e202108018.

990 **Wang, J. T. and Stearns, T.** (2017). The ABCs of Centriole Architecture: The Form and
991 Function of Triplet Microtubules. *Cold Spring Harb Symp Quant Biol* **82**, 145–155.
992 **Wang, W.-J., Acehan, D., Kao, C.-H., Jane, W.-N., Uryu, K. and Tsou, M.-F. B.** (2015). De
993 novo centriole formation in human cells is error-prone and does not require SAS-6 self-
994 assembly. *eLife* **4**, e10586.
995 **Wang, J. T., Kong, D., Hoerner, C. R., Loncarek, J. and Stearns, T.** (2017). Centriole triplet
996 microtubules are required for stable centriole formation and inheritance in human cells.
997 *eLife* **6**, e29061.
998 **Woglar, A., Pierron, M., Schneider, F. Z., Jha, K., Busso, C. and Gönczy, P.** (2022).
999 Molecular architecture of the C. elegans centriole. *PLoS Biol* **20**, e3001784.
1000 **Zhang, Y., Vanoli, F., LaRocque, J. R., Krawczyk, P. M. and Jasin, M.** (2014). Biallelic
1001 targeting of expressed genes in mouse embryonic stem cells using the Cas9 system.
1002 *Methods* **69**, 171–178.

Figure 1

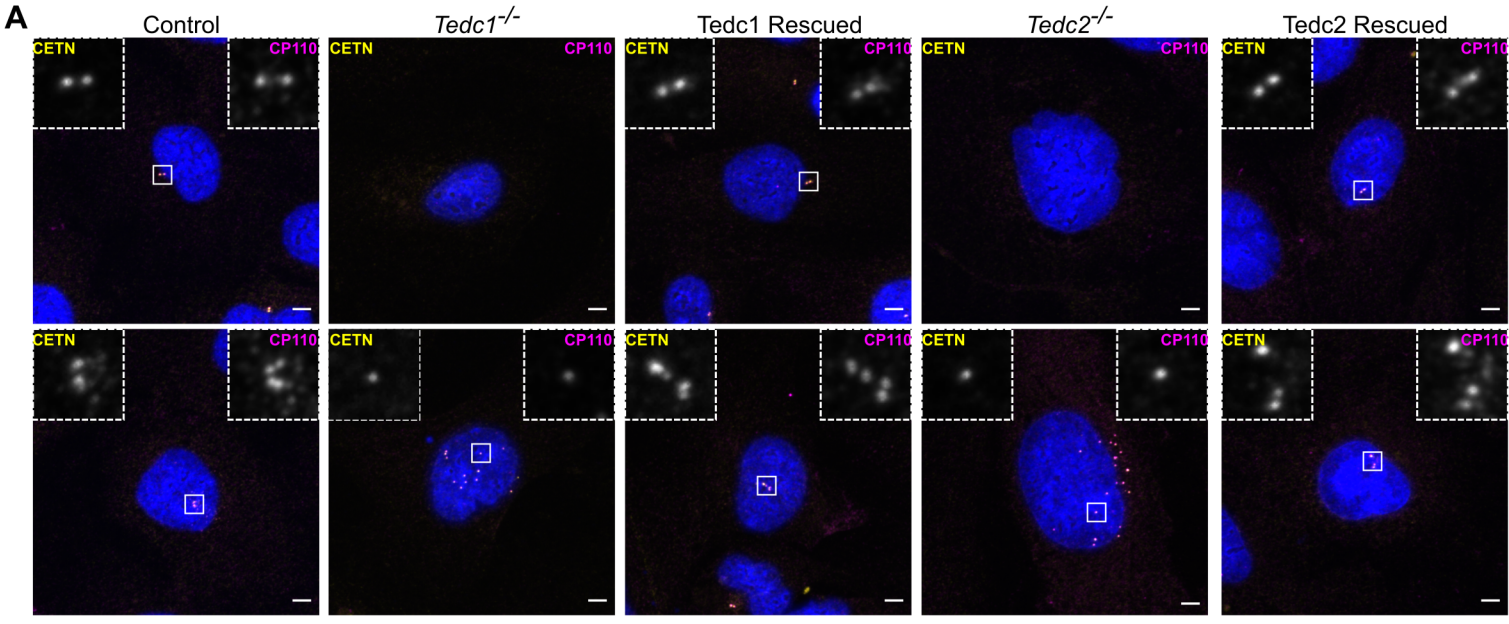
A
Control
Tedc1-/-
Tedc1 Rescued
Tedc2-/-
Tedc2 Rescued
CETN
CP110

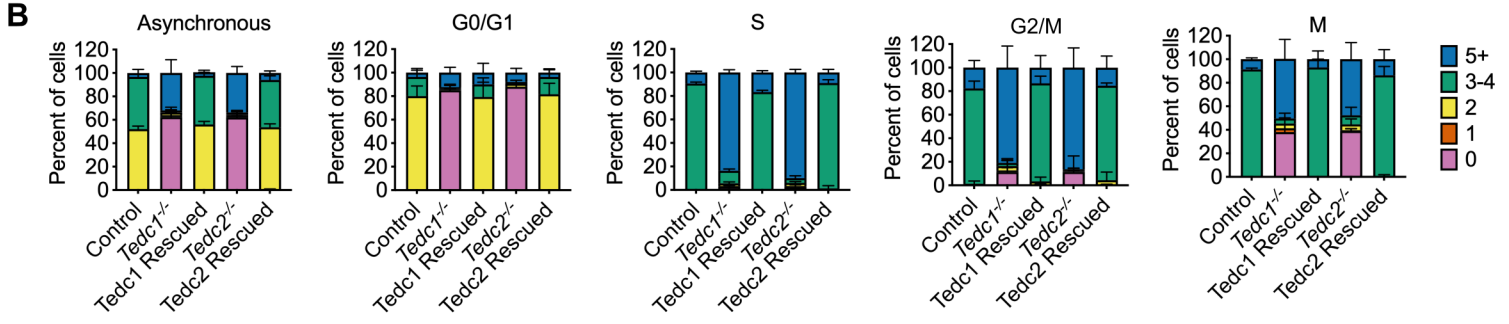
B
Asynchronous
G0/G1
S
G2/M
M
Percent of cells
Control
Tedc1-/-
Tedc1 Rescued
Tedc2-/-
Tedc2 Rescued
5+
3-4
2
1
0

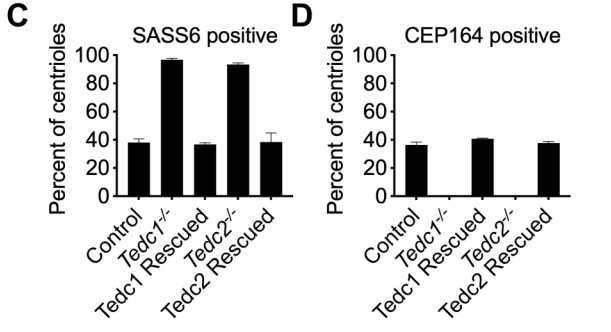
C
SASS6 positive
D
CEP164 positive
Percent of centrioles
Control
Tedc1-/-
Tedc1 Rescued
Tedc2-/-
Tedc2 Rescued

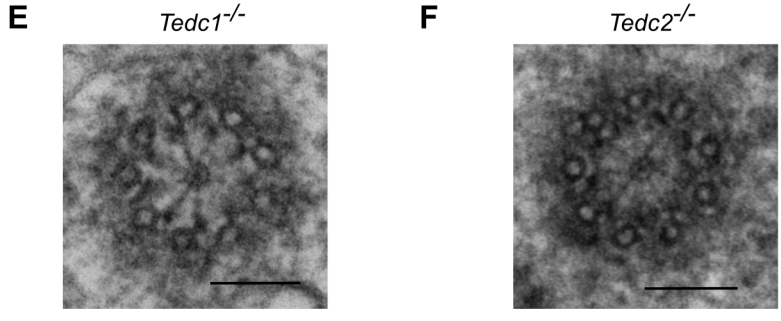
E
Tedc1-/-
F
Tedc2-/-

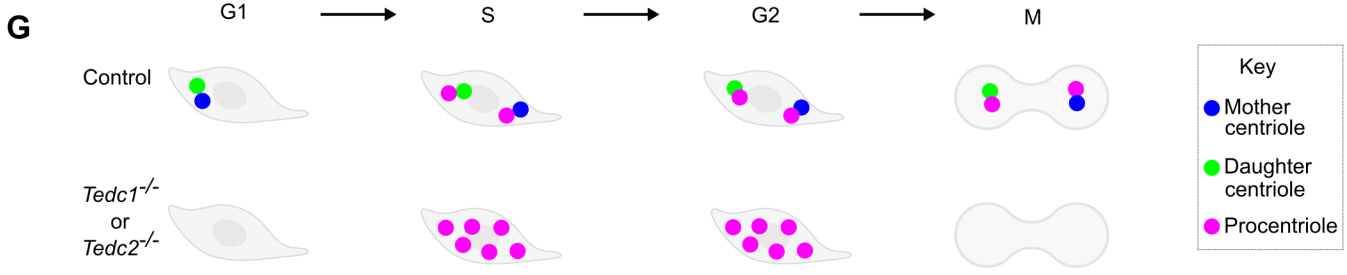
G
G1
S
G2
M
Control
Tedc1-/-
or
Tedc2-/-
Key
Mother centriole
Daughter centriole
Procentriole

Figure 1 - Supp 1

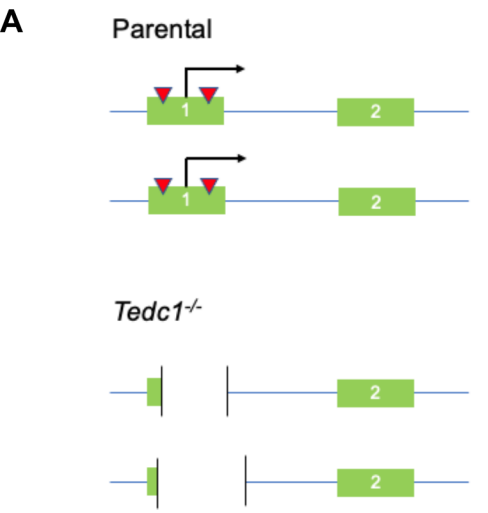

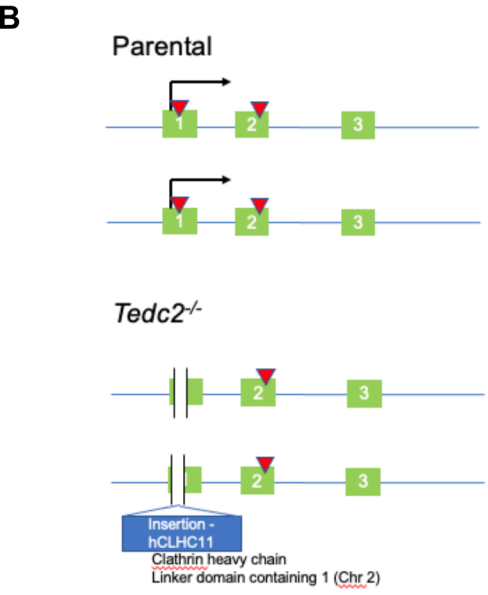

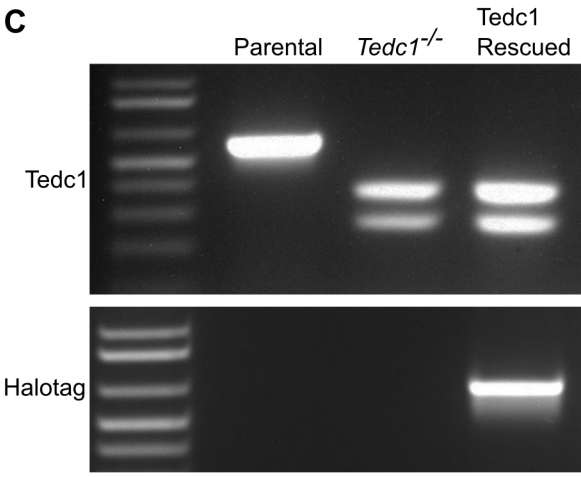

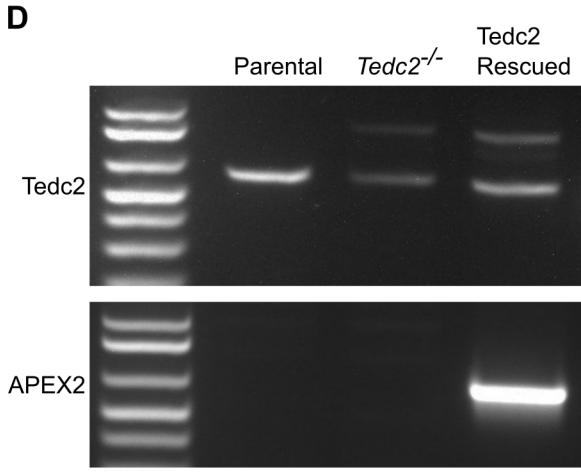

Figure 2

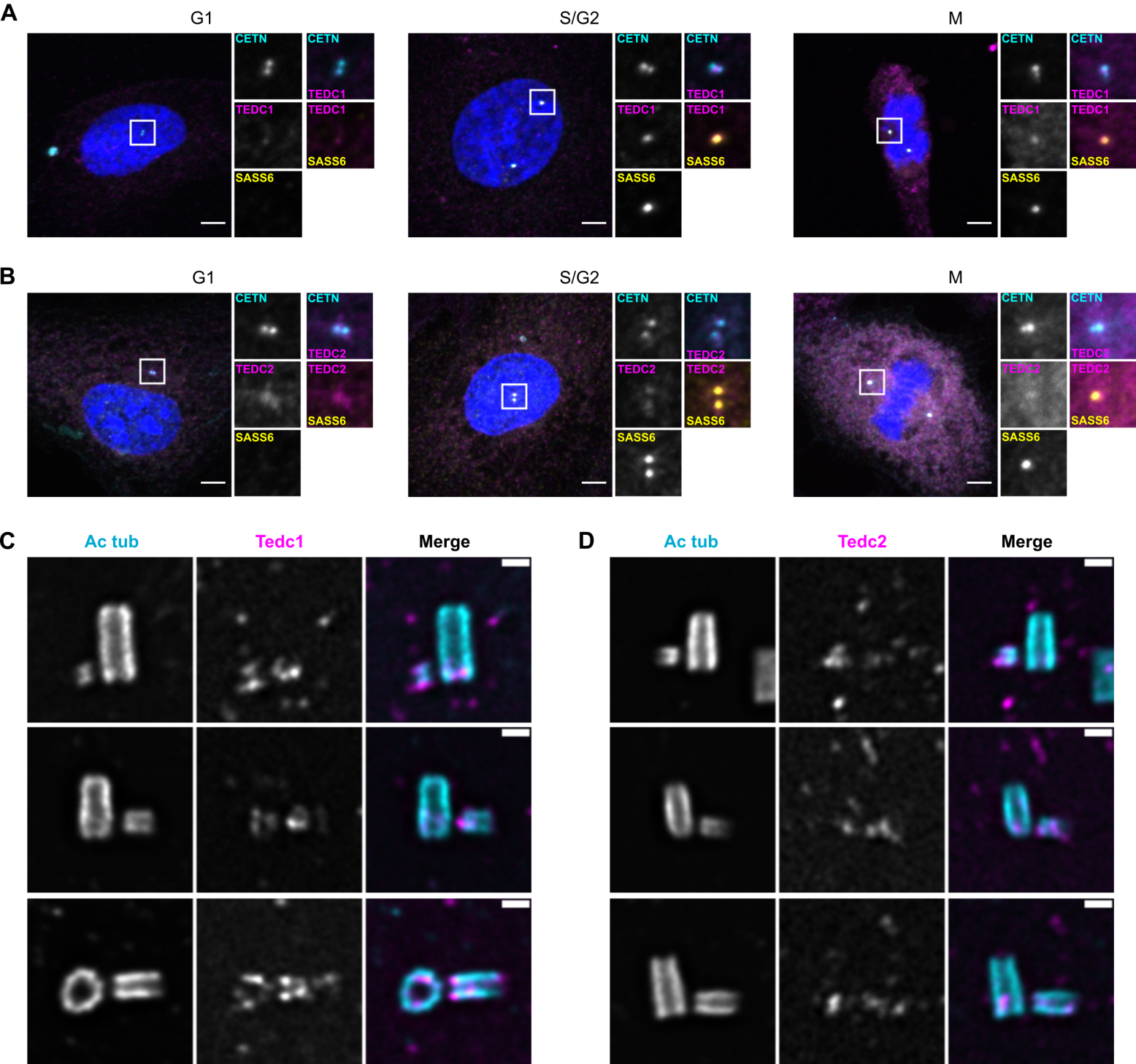

Figure 2 - Supp 1

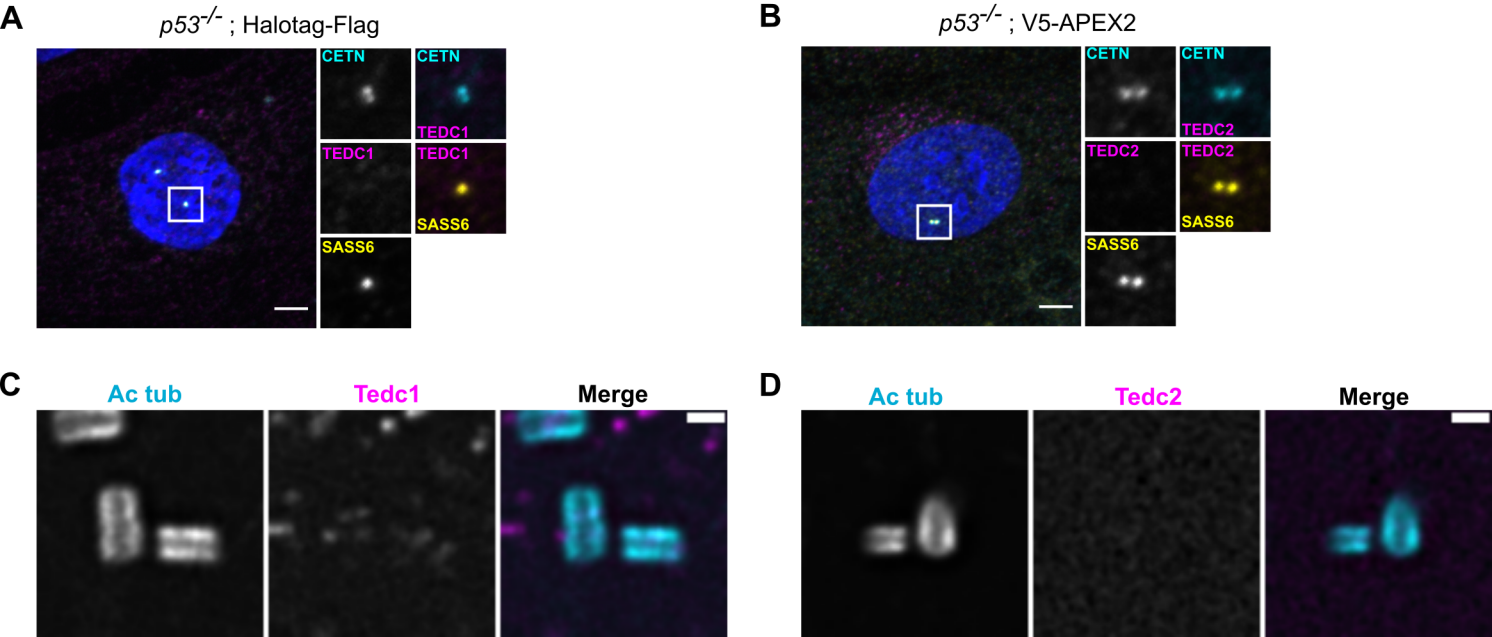

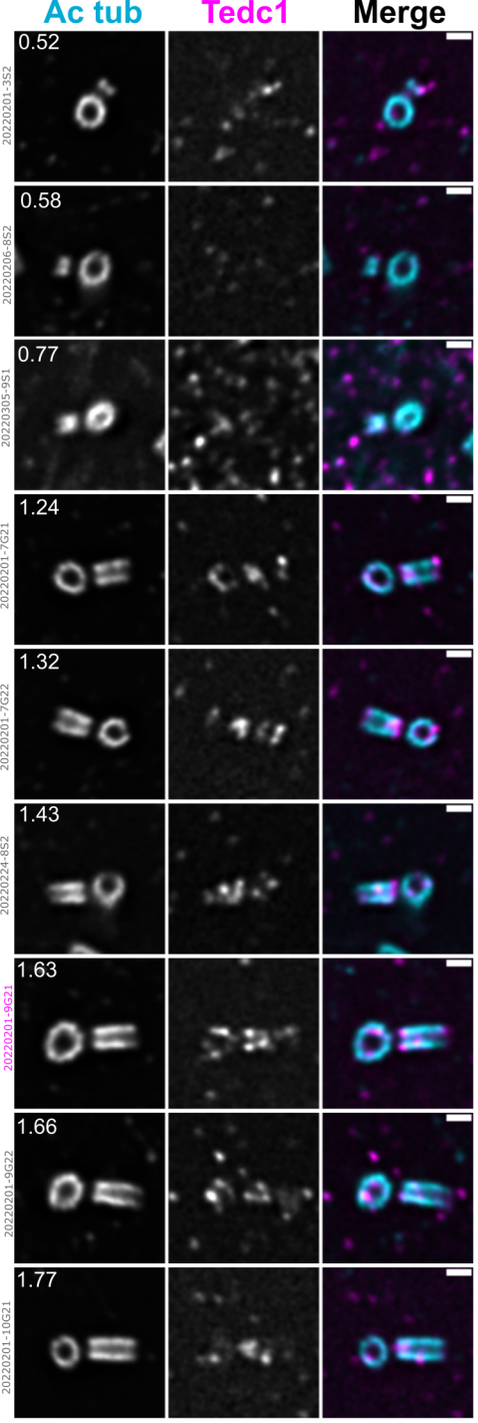

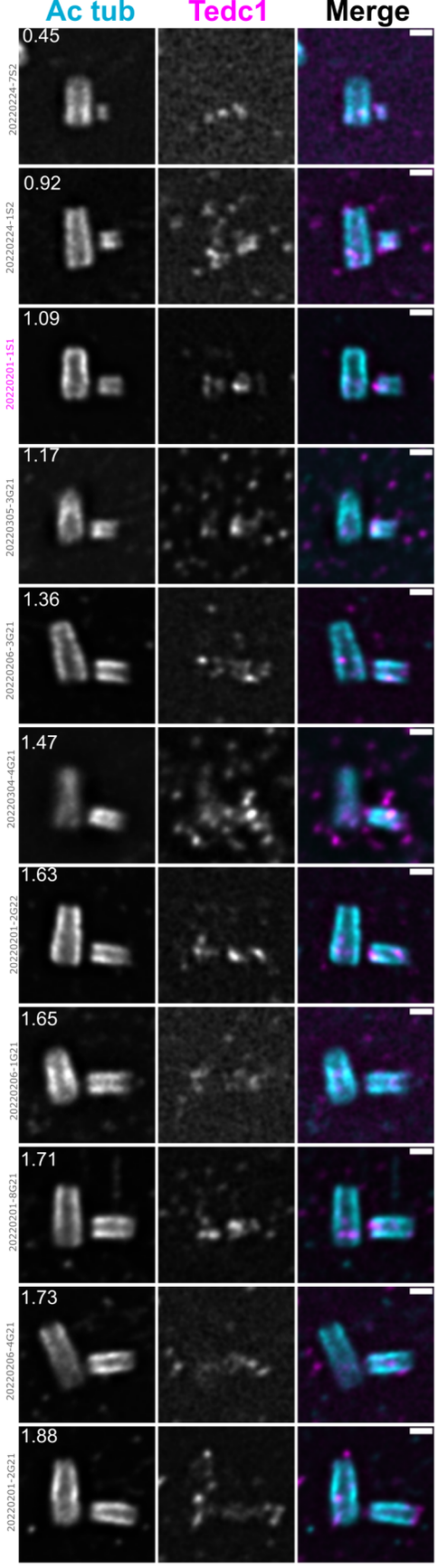

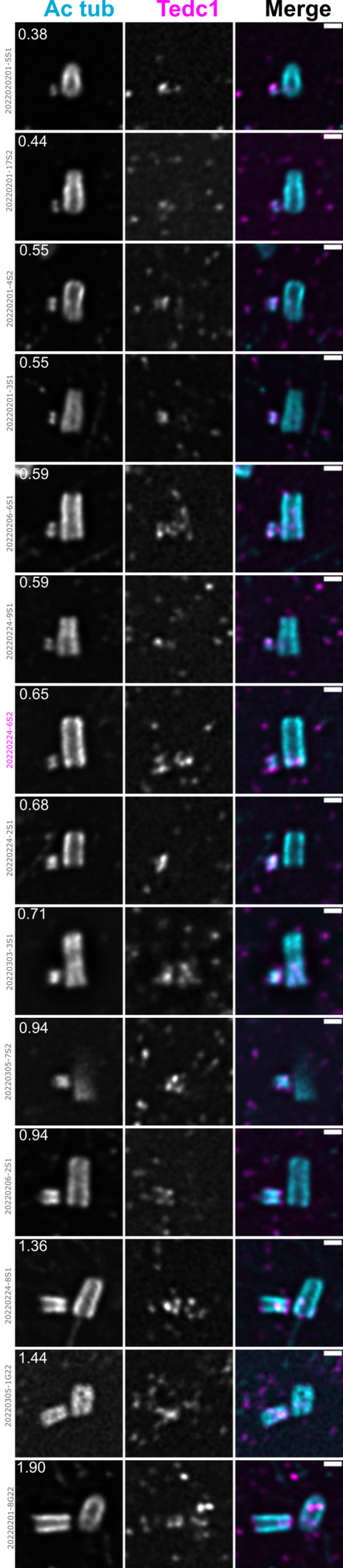

Figure 2 - Supp 2

Figure 2 - Supp 3

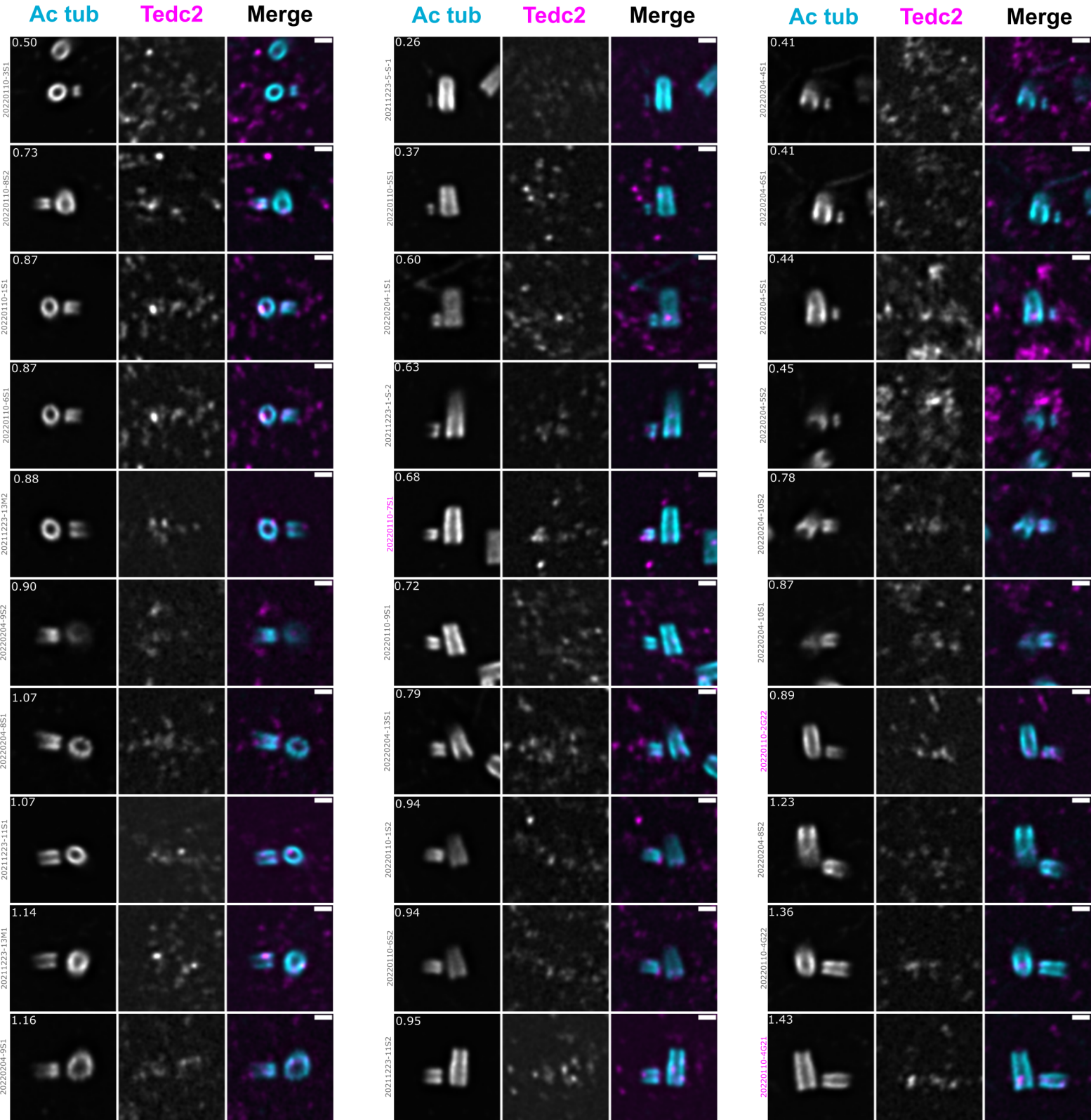

Figure 3

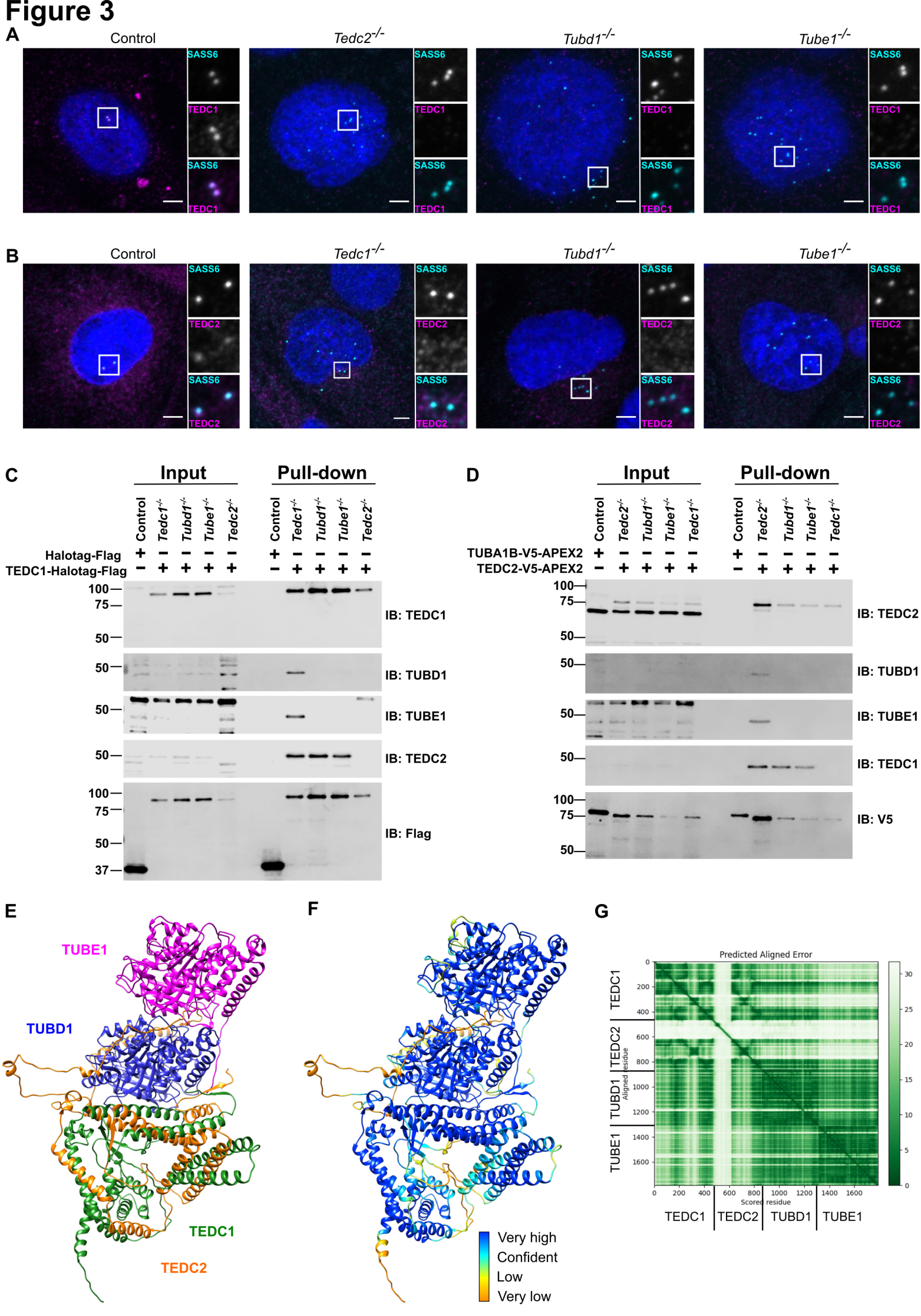
A
Control
Tedc2-/-
Tubd1-/-
Tube1-/-
SASS6
TEDC1
B
Control
Tedc1-/-
Tubd1-/-
Tube1-/-
SASS6
TEDC2
C
Input
Pull-down
Control
Tedc1-/-
Tubd1-/-
Tube1-/-
Tedc2-/-
Halotag-Flag
TEDC1-Halotag-Flag
IB: TEDC1
IB: TUBD1
IB: TUBE1
IB: TEDC2
IB: Flag
100
75
50
37
D
Input
Pull-down
Control
Tedc2-/-
Tubd1-/-
Tube1-/-
Tedc1-/-
TUBA1B-V5-APEX2
TEDC2-V5-APEX2
IB: TEDC2
IB: TUBD1
IB: TUBE1
IB: TEDC1
IB: V5
100
75
50
E
TUBE1
TUBD1
TEDC1
TEDC2
F
Very high
Confident
Low
Very low
G
Predicted Aligned Error
Aligned residue
Scored residue
TEDC1
TEDC2
TUBD1
TUBE1
0
200
400
600
800
1000
1200
1400
1600
30
25
20
15
10
5
0

Figure 3 - Supp 1

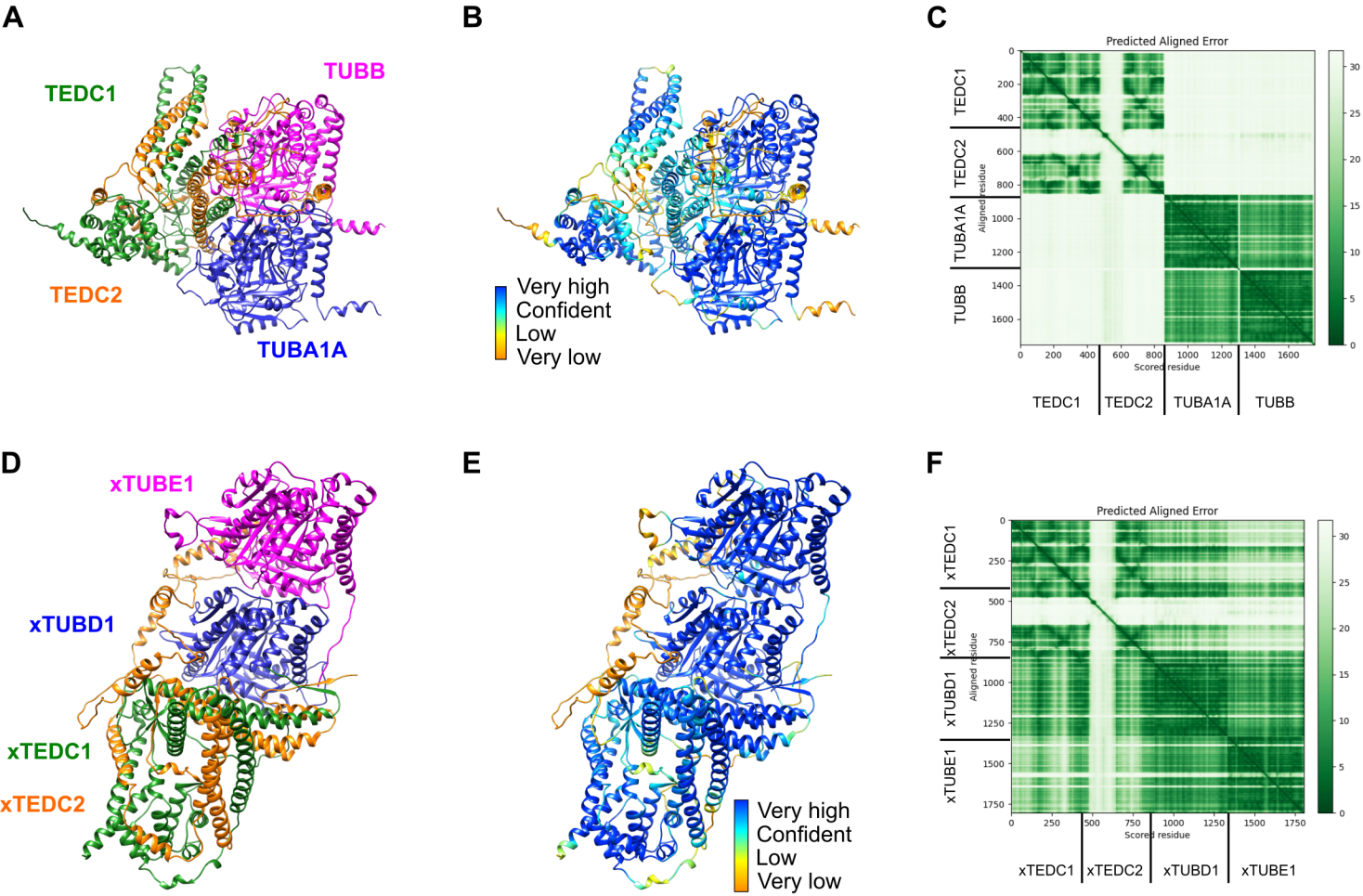

Figure 4

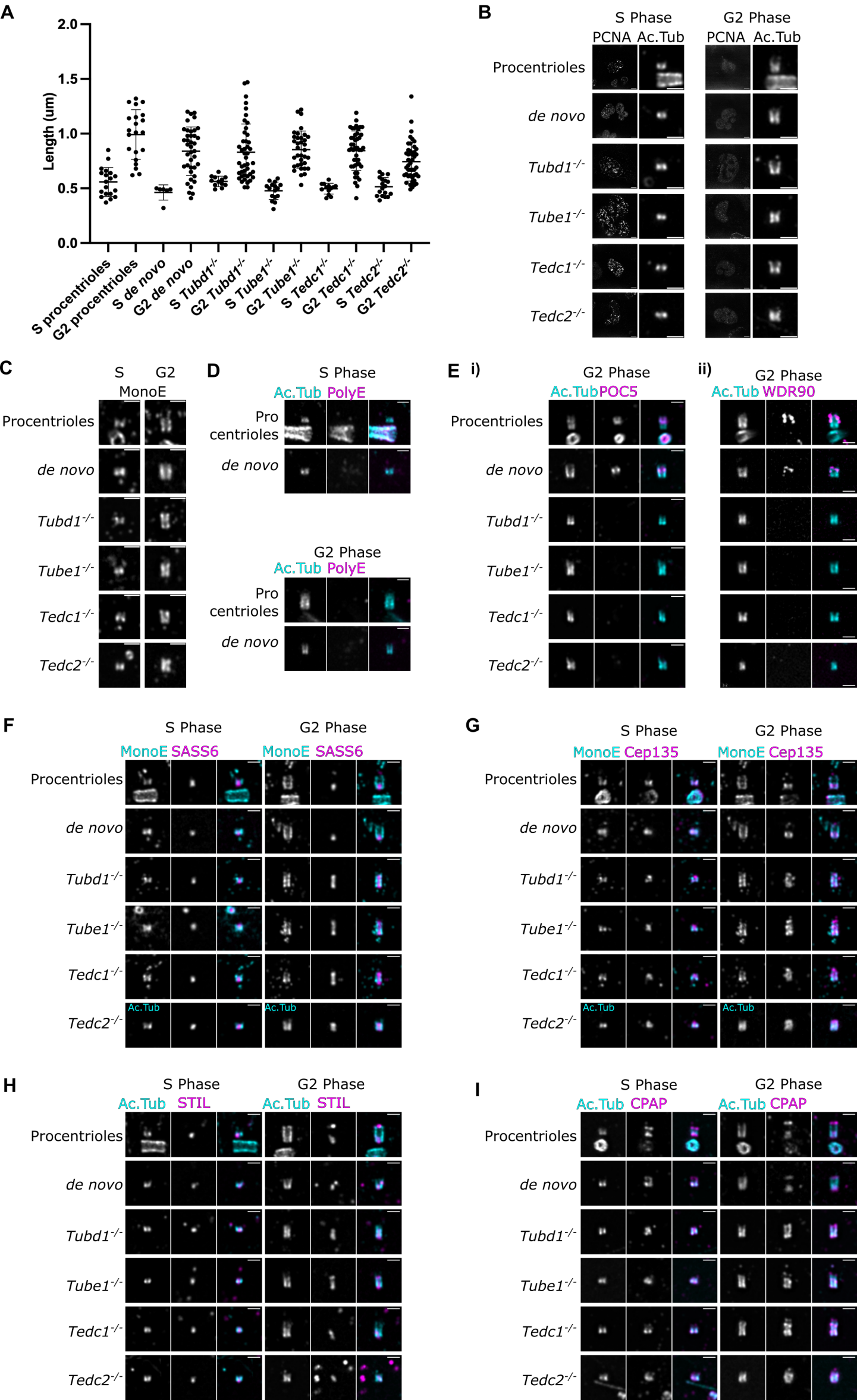
A
Length (um)
2.0
1.5
1.0
0.5
0.0
S procentrioles
G2 procentrioles
S de novo
G2 de novo
S Tubd1-/-
G2 Tubd1-/-
S Tube1-/-
G2 Tube1-/-
S Tedc1-/-
G2 Tedc1-/-
S Tedc2-/-
G2 Tedc2-/-
B
S Phase
G2 Phase
PCNA Ac.Tub
PCNA Ac.Tub
Procentrioles
de novo
Tubd1-/-
Tube1-/-
Tedc1-/-
Tedc2-/-
C
S
G2
MonoE
Procentrioles
de novo
Tubd1-/-
Tube1-/-
Tedc1-/-
Tedc2-/-
D
S Phase
Ac.Tub PolyE
Pro centrioles
de novo
G2 Phase
Ac.Tub PolyE
Pro centrioles
de novo
E
i)
G2 Phase
Ac.Tub POC5
ii)
G2 Phase
Ac.Tub WDR90
Procentrioles
de novo
Tubd1-/-
Tube1-/-
Tedc1-/-
Tedc2-/-
F
S Phase
G2 Phase
MonoE SASS6
MonoE SASS6
Procentrioles
de novo
Tubd1-/-
Tube1-/-
Tedc1-/-
Tedc2-/-
Ac.Tub
Ac.Tub
G
S Phase
G2 Phase
MonoE Cep135
MonoE Cep135
Procentrioles
de novo
Tubd1-/-
Tube1-/-
Tedc1-/-
Tedc2-/-
Ac.Tub
Ac.Tub
H
S Phase
G2 Phase
Ac.Tub STIL
Ac.Tub STIL
Procentrioles
de novo
Tubd1-/-
Tube1-/-
Tedc1-/-
Tedc2-/-
I
S Phase
G2 Phase
Ac.Tub CPAP
Ac.Tub CPAP
Procentrioles
de novo
Tubd1-/-
Tube1-/-
Tedc1-/-
Tedc2-/-

Figure 4 - Supp 1

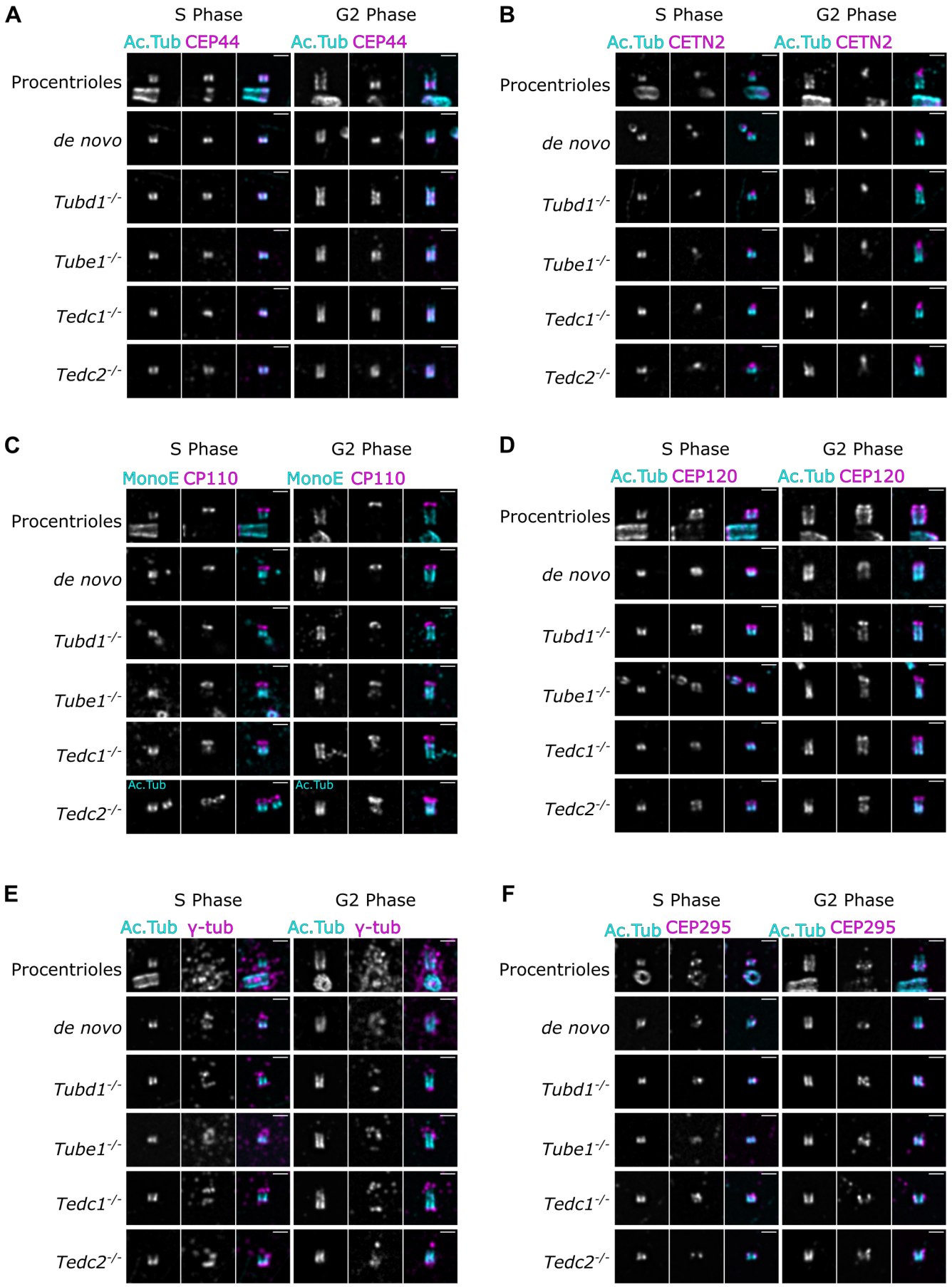

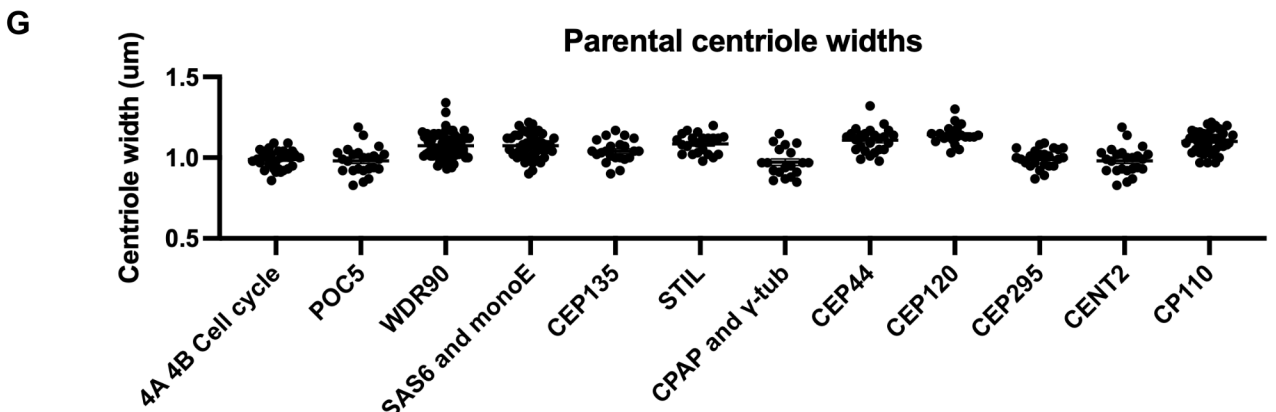

Figure 4 - Supp 2

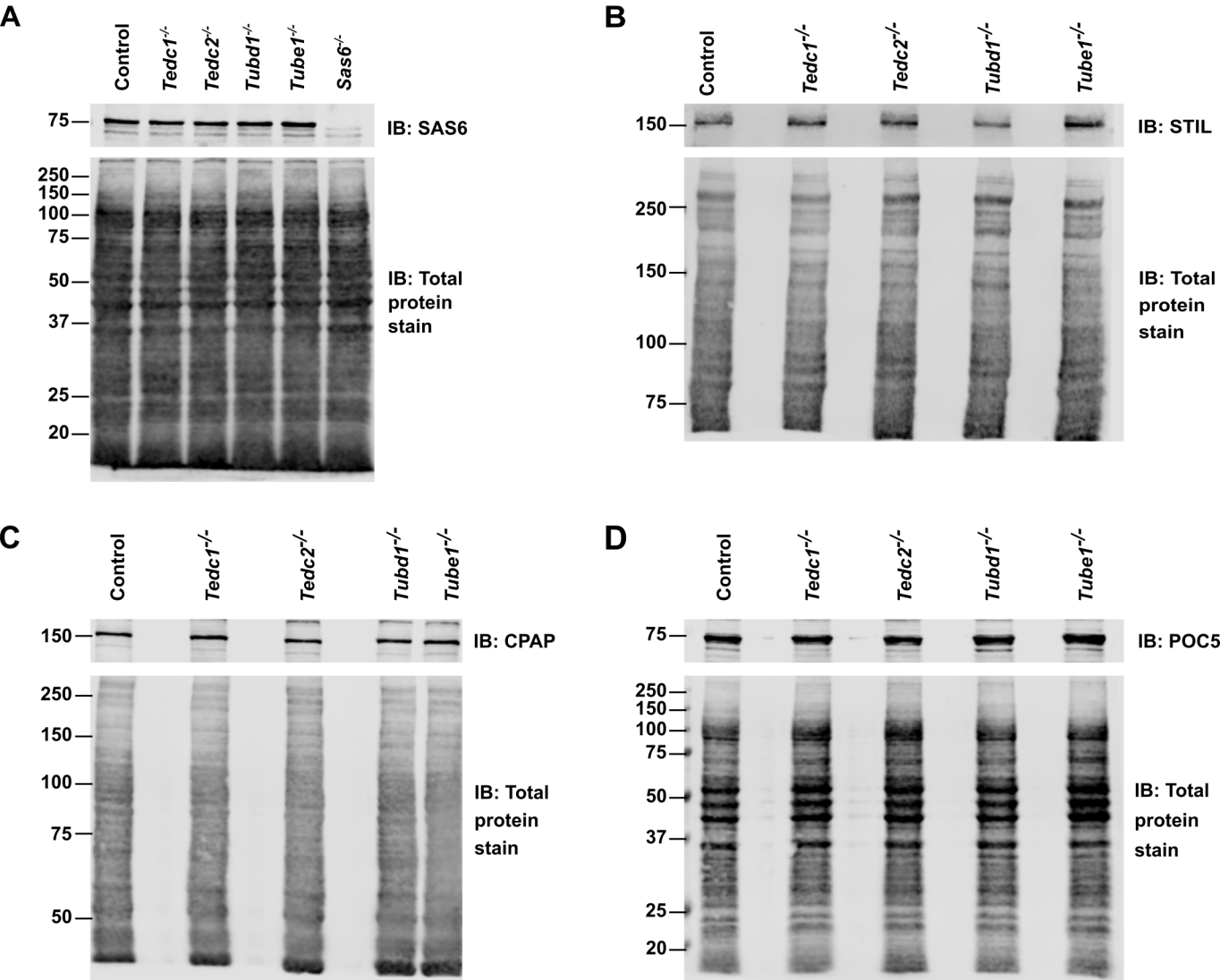

Figure 5

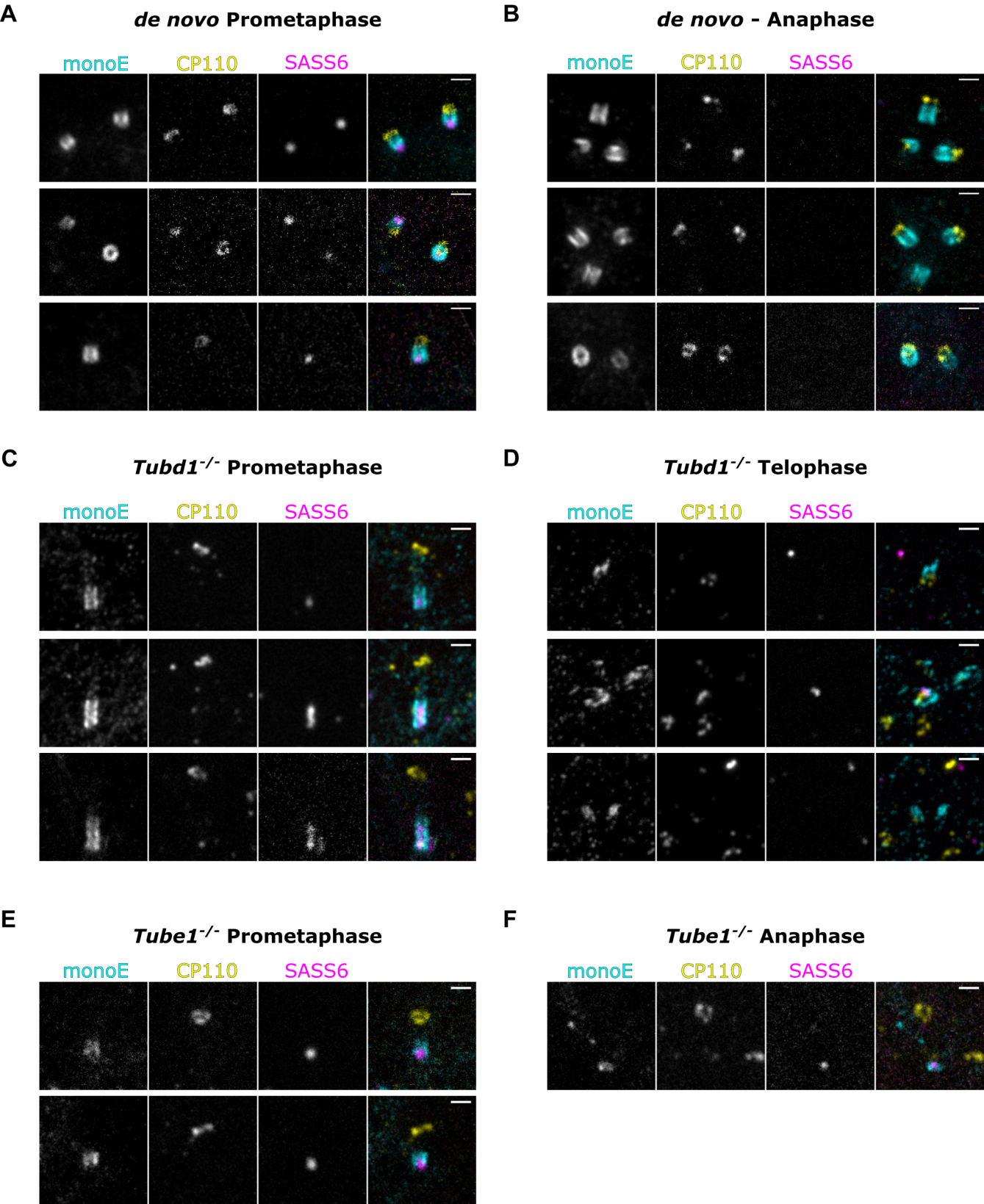
A
de novo Prometaphase
monoE
CP110
SASS6
B
de novo - Anaphase
monoE
CP110
SASS6
C
Tubd1$^{-/-}$ Prometaphase
monoE
CP110
SASS6
D
Tubd1$^{-/-}$ Telophase
monoE
CP110
SASS6
E
Tube1$^{-/-}$ Prometaphase
monoE
CP110
SASS6
F
Tube1$^{-/-}$ Anaphase
monoE
CP110
SASS6